Detailed Design of a Pulsed Plasma Thrust Stand

by

Andrew J. Verbin

A Thesis Presented in Partial Fulfillment
of the Requirements for the Degree
Master of Science

Approved April 2017 by the
Graduate Supervisory Committee:

Timothy Takahashi, Co-Chair
Daniel B. White, Co-Chair
Konrad Rykaczewski

ARIZONA STATE UNIVERSITY

May 2017

ABSTRACT

This thesis gives a detailed design process for a pulsed type thruster. The thrust stand designed in this paper is for a Pulsed Plasma Thruster built by Sun Devil Satellite Laboratory, a student organization at Arizona State University. The thrust stand uses a torsional beam rotating to record displacement. This information, along with impulse-momentum theorem is applied to find the impulse bit of the thruster, which varies largely from other designs which focus on using the natural dynamics of the fixtures. The target impulse to record on this fixture was estimated to be 275 μN-s of impulse. Through calibration and experimentation, the fixture is capable of recording an impulse of 332 μN-s ± 14.81 μN-s, close to the target impulse. The error due to noise was characterized and evaluated to be under 5% which is deemed to be acceptable.

DEDICATION

I'd like to dedicate this paper to my parents and family, both the Verbin and the Hardy families, without their love and support I would never have been able to make it this far in life or my education. I would also like to especially dedicate this work to my uncle, Steve Hardy, who always loved talking about math and engineering with me when no one else understood what we were talking about, which always made us laugh.

ACKNOWLEDGMENTS

Mr. Verbin performed this research in partial fulfillment of the degree requirements for obtaining his M.S. in Aerospace Engineering from Arizona State University. All analysis was completed at Arizona State University. Mr. Verbin was supported by his two thesis co-chairs, Dr. Timothy Takahashi and Dr. Daniel White. He would also like to thank Air Devils for allowing the use of materials and tools. Finally, thanks to Don Wood for welding components and the suggestion of the ball rod end.

TABLE OF CONTENTS

Page

Page

LIST OF TABLES

Table Page

LIST OF FIGURES

Figure Page

Figure Page

NOMENCLATURE

A	=	amplitude of displacement
a	=	thruster footprint length
$\vec{B}$	=	magnetic field
b	=	thruster footprint width
$\vec{F}$	=	force vector
F_{th}	=	force of thrust
g	=	gravity
h	=	height of release of calibration weight
I	=	mass moment-of-inertia
I_b	=	impulse bit
$I_{b,c}$	=	impulse bit of calibration weight
I_{roll}	=	mass moment-of-inertia in roll
I_{th}	=	thruster mass moment-of-inertia
I_{yaw}	=	mass moment-of-inertia in yaw
J	=	torsional arm moment-of-inertia
$\vec{J}$	=	current density
L	=	angular momentum
$L_{calibration}$	=	angular momentum of calibration weight
L_{stand}	=	angular momentum of thrust stand
l_{arm}	=	arm length from pivot point to LVDT
l_{cw}	=	arm length from pivot point to counterweight (horizontal)
$l_{cw,z}$	=	arm length from pivot point to counterweight (vertical)

l_{th} = arm length from pivot point to thrust vector

LVDT = linear variable displacement transformer

m = mass

$m_{calibration}$ = mass of calibration pendulum

m_{cw} = mass of counterweight

m_{th} = mass of thruster

P = linear momentum

$P_{calibration}$ = linear momentum of calibration pendulum

P_{c1} = linear momentum of calibration weight at position 1

P_{c2} = linear momentum of calibration weight at position 2

ΔP_c = change of linear momentum of calibration weight

PPT = pulsed plasma thruster

r = radius

r_{LVDT} = radius of rotation at LVDT

r_{th} = radius of rotation at thrust line

t = time (s)

Δt = pulse time

v = linear velocity

v_{LVDT} = linear velocity at LVDT

x(t) = displacement

α = displacement angle (roll)

γ = displacement angle (pitch)

ζ = damping coefficient

θ = displacement angle (yaw)

ω = angular frequency

I. INTRODUCTION

Pulsed plasma thrusters (PPT) have been used in many applications over many years in spacecraft propulsion. They can be used as the primary propulsion for a small craft such as canisterized spacecraft like those conforming to the CubeSat standard. They can also be used as attitude and control thrusters in order to reorient a medium sized satellite or other type of craft. Lastly, PPTs could be used to station keep a satellite from orbital perturbations.

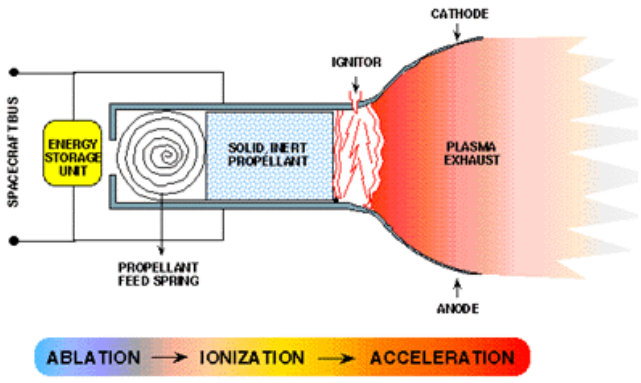

Fig. 1 Basic PPT configuration

A PPT, pictured in Fig. 1, is a relatively simple device in its design. The thruster assembly is comprised of a capacitor bank connected to a pair of electrodes. A spark plug initiates the capacitor discharge; the resulting arc ablates and ionizes the PTFE (Teflon) propellant. Thrust is produced in the axial direction, perpendicular to the current density and the induced magnetic field, according to the vector cross product:

$$\vec{F} = \vec{J} \times \vec{B}$$

These types of thrusters are a part of a class of pulsed-mode electromagnetic devices. They typically discharge over $10^{-5} – 10^{-6}$ sec, the pulse frequency can be varied to achieve a desired average thrust, consistent with the available mean operating power. While the achieved impulse bit per cycle varies according to thruster design, typical values of impulse bit are in the range of $10^{-6} – 10^{-3}$ N-s.

This extremely short firing time makes certain measurements, including thrust and impulse, difficult to accomplish because there is no steady state firing mode. A thrust test stand must be able to record the impulse delivered in an extremely short amount of time. Due to the delivered impulse capabilities, the thrust stand must be able to measure that small impulse either directly or indirectly, as will be explained later.

Generally, there are a few different types of thrust stands including torsional and pendulum (both inverted and normal pendulum) configurations. Each type of thrust stand has certain advantages and disadvantages. A torsional style thrust stand will typically be a short device but have a larger footprint in the vacuum chamber due to the needed length of the torsional arm in order to appropriately react to the extremely low amount of thrust developed by the PPT. A pendulum configuration would have a smaller standing footprint in the vacuum chamber because the swinging arm length is vertically long, the platforms wouldn’t need to be large (depending on the size of the thruster and counterweights), but would be quite tall.

The thrust stand designed for this thesis is one that follows the torsional type as seen in Fig. 2; it will use a knife edge bearing or pivot point along the same lines as a tone arm on a record player. This design choice is made in order to reduce friction to as close to zero as possible. In order to design an effective thrust stand, there are a few things that need to be calculated or taken into account: the mass moments-of-inertia in all three directions (yaw, pitch, and roll), as well as the relevant frequency modes. The reasoning behind this will be discussed further in this thesis.

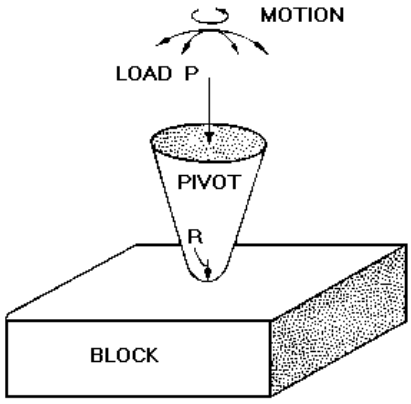

Fig. 2 Showing an example of a knife edge pivot point

In order to measure the thrust of the PPT a linear variable displacement transformer (LVDT) measures the displacement of the torsional arm. The reasoning and calculations to infer impulse from position history will be discussed later on in this thesis.

II. PRIOR WORK

Early in the development of electric propulsion devices, engineers recognized a need to measure low thrust or impulse bit values typical of conventional electric thrusters. As per its name, a thrust stand measures thrust or the force imparted on an object by the thruster in order to move the spacecraft. A simple measurement solution would employ some sort of a force transducer to record the data. Unfortunately it is difficult to directly use a force transducer since the pulse of force occurs across such a small time period that requires extremely precise and high sampling rate sensor operating on a massless thruster. Another approach for pulsed thrusters is to measure total impulse; from there, the engineer can infer the force of thrust created by the PPT.

Due to the extensive flight heritage of the PPT, there have been a number of successful designs for ground-based measurement systems used to obtain high fidelity thrust measurement data. The first PPT was used onboard the Zond 2 spacecraft in 1964 by the USSR and on the LES-6 spacecraft by the United States in 1968[1]. Since then it has been used extensively in the field of space propulsion.

Engineers developed a number of different thrust stands aimed at pulsed firing type thrusters. This section aims to show some of those designs and pull from them the important design features inherent to them. In previous work, there is a paucity of in depth design detail. Previous work concentrates on characterization of thruster design, performance and operation. This work documents our approach to the detail design of a test fixture.

A. Conceptual Design Requirements

In order for the thrust stand to effectively record its measurements, it must meet some design requirements. These requirements include both mechanical design and recordable data constraints.

Since the thrust stand design undertaken in this work involves a knife edge pivot bearing, the mechanism must first be statically balanced in three axes of pitch, roll, and yaw. Essentially the torsional arm balances on a sharp point. This is necessary to make it as close as possible to being frictionless (in order for the thrust measurements to be accurate and to not lose energy). Also, the torsional arm must be balance with the thruster attached at a far end. It must statically balance the thruster with a counterweight affixed to the other side of the pivot point.

Additionally, since the pivot point can move in any direction or plane, such as yaw, pitch, and roll, or any combination of the three, the fixture was engineered such that the mass moments of inertia in all three directions resulted in a yawing mass moment-of-inertia that is a few orders of magnitude smaller than roll. This was done in order to reduce the error possible from thrust vector misalignments. If the thrust vector is slightly off from horizontal and the mass moments of inertia are calibrated correctly, the torsional arm will want to move in the yawing plane more than the others. This keeps the torsional arms movement in the horizontal plane, and thus give good displacement data from which to infer impulse.

Due to the need for the movement of the torsional arm to be linear (explained further in this section) the movement of the arm will need to be restricted in its allowable total deflection but must be applied in a way that the damping of the arm remains negligible. This is accomplished by one of two solutions: 1) either implementing extremely weak springs near the pivot point or 2) using weak magnets. These, if placed within a certain distance on each side of the torsional arm from the pivot point, will restrict the arms deflection angle to keep it in the realm of small angle approximation and center the torsional arm after its initial deflection. They will be weak enough that the centering force will be negligible compared to the force given by the thruster.

The data that will be recorded from the torsional arm is its displacement. This is accomplished using a LVDT (the description of its internal functions is explained further on in the paper). The displacement that is able to be recorded must be linear, thus the torsional arms displacement needs to be rendered as linear motion. If the displacement angle of the torsional arm is kept to a small enough angle the small angle approximation can be used and the angle of displacement is approximated to the linear displacement, the data recorded by the LVDT. As will be discussed later, this displacement data will be used along with other information to calculate the thrust.

B. Thrust Stand Design – Pendulum or Torsional

The first design parameter that will be investigated will be the overall configuration of the stand i.e. torsional or pendulum. Both thrust stand types include a pivot point, counterweight and thruster. The different between the two is a torsional thrust stand pivots

in the horizontal plane (yawing) while a pendulum thrust stand pivots along a vertical plane (pitching). It is important to look at how others have used these designs and how they compare to the proposed design in this paper.

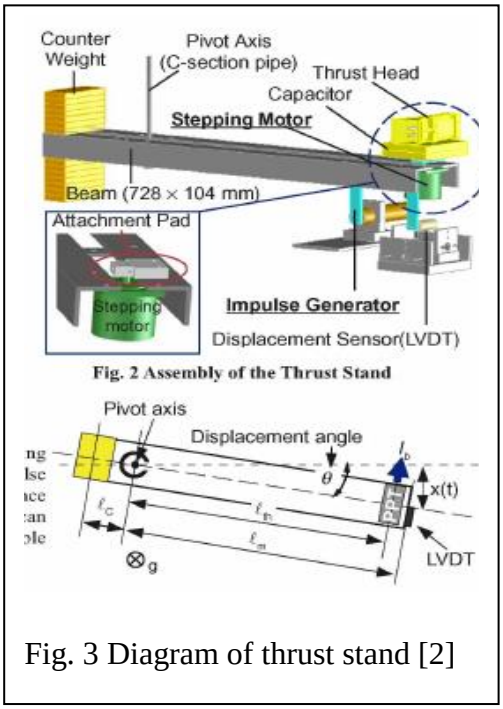

Fig. 3 Diagram of thrust stand [2]

The first thrust stand design evaluated, [2] shown in Fig. 3, is that of a torsional beam style. This type of thrust stand has the thruster on one end of a beam, and some kind of counterweight on the other end in order to keep the beam balanced. It spins about a pivot axis placed somewhere between the thruster and counterweight. This particular design also investigated the uses of thruster vectoring using a stepping motor to change the direction of the thruster head on the stand but that is not important to the design in this case.

As can be deduced from Fig. 3 (previous page), the total length of the torsional arm is 728 mm long. The paper does not give the lengths of the arm to the thruster from the pivot point or the length to the counterweights from the pivot point. In the paper, it is described that "the length of l_m and l_{th} must be sufficiently longer than l_c".

The pivot point is described as a C-section of pipe with a sufficiently small torsional spring constant. There is no description on how this property was calibrated or proven to be small enough to not affect the thrusters' ability to push the torsional beam to get the needed data.

This thrust stand uses a LVDT to record the displacement of the torsional arm. If the torsional arm is limited to a small enough angle of displacement the displacement is linear and thus can be recorded by the LVDT.

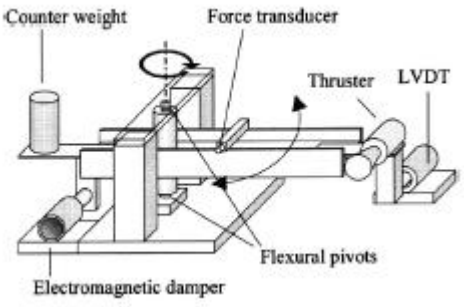

Fig. 4 Diagram of thrust stand [3]

As can be seen in Fig. 4 [3], a torsional design is used for the stand. The thruster on one end of the beam, counterweight on the other to keep the torque arm balanced and level and

a pivot point somewhere in between to allow the stand to spin when the thruster is fired. This design in its most basic form is very similar to the design for Fig. 3, including its use of a LVDT for the data recording device.

The paper is light on the details of the dimensions for the torsional arm. The arm is mentioned to be statically balanced using counterweights. Though it does not mention the actual distances of the thruster or counterweights from the pivot point. Additionally, it mentions the natural period of motion to be 4-5 seconds.

The difference between this thrust stand and the previous one is the use of a component called flexural pivots. Flexural pivots are a frictionless bearing that require no lubricant of any kind and thus can be used in small movements and a vacuum chamber. These flexural pivots have an inherent torsional spring stiffness. There are no calculations proving the stiffness in the flexural pivots won't overwhelm the thrust from the thruster. The stand does use an electromagnetic damper but this device is only used while the thruster is not firing so there will be no effect on the electromagnetic field of the thruster.

The design of the thrust stand in Fig. 5 [4] (overleaf) is described as a "torsional thrust stand". Though it is difficult to see but the thruster, pivot points and counterweights can be noted by their labels. Again, this design at its core is similar to the other designs mentioned above. It can be noted that the torsional style stand is showing to be the popular of the two design types.

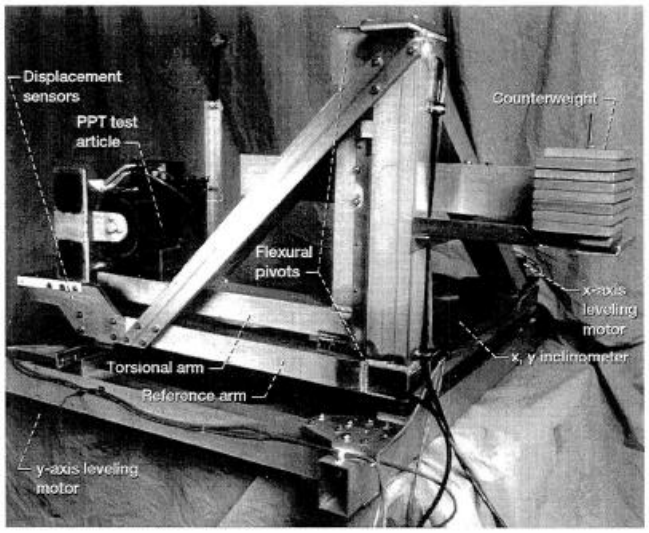

Fig. 5 Diagram of thrust stand [4]

The paper gives some of the dimensions of the torsional arm unlike some of the other papers. The thruster is placed 0.59 meters from the pivot point. Though it doesn't cover the distance or mass of the counterweights. This design, similar to the above thrust stand, uses flexural pivots. There is no description of how the flexural pivots were chosen or how the flexural pivots wouldn't overwhelm the thruster's ability to move the torsional arm.

The next thrust stand, Fig. 6 [5] (overleaf), is classified as a pendulum style, similar to something called "Watt's Pendulum". The design is used in a fashion such that it moves in a straight-line motion. Its mechanism is described as a

> "horizontal bar supported at one end by a hinged lever and is suspended as the other end by a flat ribbon of spring steel.

The ribbon in turn is hinged in the middle by a short length of spring stock turned at right angles to give the entire suspension lateral freedom. With the lever and ribbon given equal length, the center of the horizontal bar moves in a straight line when pushed through its axis." [5]

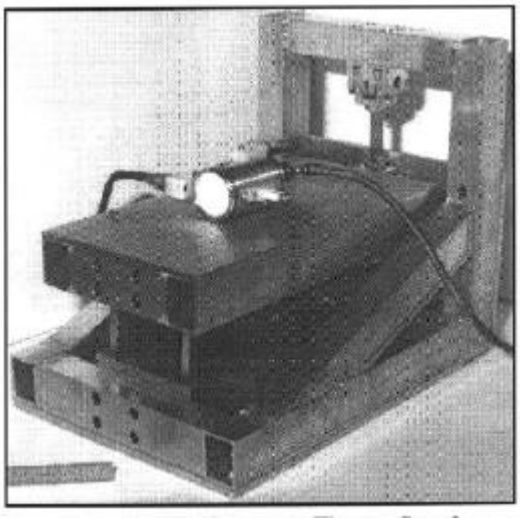

Fig. 6 Picture of thrust stand [5]

Again, like the previous papers, this paper gives little detail on the calculation and sizing of the pendulum lengths. It gives information on center of gravity calculations for stability and the period of the pendulum. Similar to the previous designs this thrust stand uses a LVDT to take displacement measurements of the horizontal displacement of the pendulum.

Looking at all of these designs, the reader can see that the more prevalent design choice is the torsional type thrust stand and the use of a LVDT for measurements. Most reports

provide little design data detailing the sizing of various structural elements, including arm lengths, and specification of flexural pivot characteristics.

For the torsional style thrust stand it is important to look at static balance, mass moments of inertia, and the dynamics of the torsional arm in order to size the arm lengths and counterweight mass among other things. But otherwise the rest of these papers on their own do not give enough information to design and construct a functional thrust stand which is the purpose of this paper.

Steady state thrusters make design of thrust stands easier because the data measurement isn't confined within a finite amount of time unlike pulsed thrusters. Pulsed thrusters (which include PPTs) have a finite time in which the thruster is operating and good data can be taken, some of these are less than a second. Thus, the thrust stand must be designed to have a large enough rotational time period to enlarge the window of opportunity to record the required data. A steady state thrust stand can use force transducers or something similar to record its data whereas pulsed thrust stands must use more ingenuity in the data measurement to get the needed data.

C. Thrust Stand Instrumentation – Position/Velocity or Force Transducer

The next important design parameter is the method of data acquisition on the thrust stand. Obviously, a thrust stand wants to measure the force of thrust developed by an engine or thruster. Mentioned earlier, a PPT leads to more complicated design of the stand since a direct force transducer cannot be used. This is due to the extremely short time frame that

the thruster fires, that the transducer doesn't have enough time to reach a steady reading to get any useful information. The previously mentioned thrust stands use a device called a LVDT to measure the linear displacement of the torsional arm or pendulum upon which the thruster is fixed. This linear displacement data can be used along with the impulse-momentum theorem to infer impulse bit data. This will be explained later in the paper.

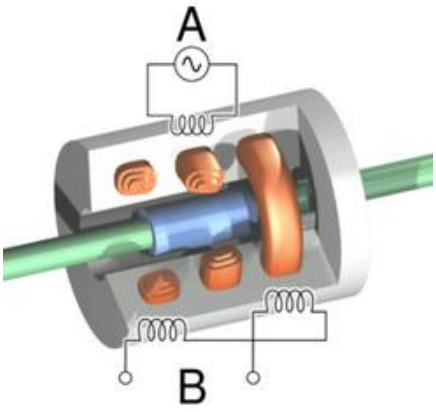

Fig. 7 Basic design of LVDT internals

A LVDT, Fig. 7, consists of three solenoidal coils, a primary coil and two secondary coils. The primary coil is the center coil while the secondary coils are on either side of the primary within the LVDT. The measurement rod has a ferromagnetic core on the end which moves through the three coils. The primary coil runs on alternating current which induces voltage in the secondary coils. When the ferromagnetic core moves it affects the induced voltages in the secondary coils which can be converted into a measured linear displacement.

Additionally, there are generally two types of LVDTs, contact and non-contact. Contact LVDTs have a small spring incorporated into the design. This spring pushes the plunger outward to the full displacement. With non-contact LVDTs the core plunger moves freely through the coils. It only moves when acted upon instead of a spring forcing movement.

This difference in LVDTs is important for the design of this thrust stand. If the LVDT has a spring in it or is a contact LVDT, it will create a resonant damping effect on the torsional arm; certain simplifications made later on cannot be made. Thus, a non-contact LVDT will be used in the design of this thrust stand.

III. THRUST STAND DYNAMICS

It is important to understand how the thrust stand will move and react to the input from the PPT firing. Thus, the dynamics of the thrust stand must be evaluated in order to understand its movement. It also determines how to infer useful data from this movement in order to find the impulse developed by the PPT.

A. Thrust stand Dynamics & Impulse Equations

The majority of prior art uses the dynamic behavior of the thrust stand to calculate the impulse of the thruster through certain assumptions and experimental knowns. The dynamics of a torsion thrust stand have been stated in the other papers to follow the second order differential equation shown in Eq. 1.

$$\ddot{\theta} + 2\zeta\omega_n\dot{\theta} + \omega_n^2\theta = \frac{I_b l_{th}}{J} \quad \text{Eq. 1}$$

Where θ is the displacement angle of the torsion arm, ζ is the damping coefficient, ω_n is the natural angular frequency of the thrust stand, I_b is the impulse bit, J is the moment-of-inertia of the entire torsional arm, l_{th} is the length of the arm from the pivot to the center of the thrust vector. This differential equation follows the solution of Eq. 2.

$$x(t) = \sin(\theta) l_{arm} = \frac{I_b l_{arm} l_{th}}{J\omega_n\sqrt{1-\zeta^2}} e^{-\zeta\omega t} \sin(\omega_n t\sqrt{1-\zeta^2}) \quad \text{Eq. 2}$$

The displacement *x(t)* can be represented as the sine of the displacement angle, θ, multiplied by the total length of the thruster arm, l_{arm}. In order for the measurement to be a linear displacement the displacement angle must be small thus we can use the small angle approximation to simplify Eq. 2 and we also must make the design to have close to no damping ratio further simplifying into Eq. 3.

$$x(t) = \theta l_{arm} = \frac{I_b l_{th} l_{arm}}{J\omega_n} \sin(\omega_n t) \quad \text{Eq. 3}$$

In order to accurately find the moment-of-inertia the best way is to apply a small pendulum to impact on the thruster arm as a calibration. To do this the equation for displacement is used, and look purely at the amplitude of the sinusoidal motion. Since the value of the amplitude is the maximum amplitude measured from the LVDT during the

impact leading to Eq. 4 which can be solved for moment-of-inertia and other known measured values.

$$A = \frac{I_b l_{th} l_{arm}}{J \omega_n} \quad \text{Eq. 4}$$

Using a small mass such as a lead weight with accurately measured mass and a known height. We know that the linear momentum of an object is governed by Eq. 5 and impulse is governed by Eq. 6.

$$P = mv = m\sqrt{2gh} \quad \text{Eq. 5}$$

Where g is gravity, h is the height of the pendulum weight and m is the mass of the weight.

$$I_{b_c} = \Delta P_c = P_{c_2} - P_{c_1} \quad \text{Eq. 6}$$

I_{bc} is the impulse of the calibration weight, since position one is the resting position the height would be zero and thus that term would cancel. Thus, the momentum of the weight imparted to the thrust stand is equal the impulse and thus can be input into Eq. 4, along with other knowns, to find moment-of-inertia of the thrust stand arm. Once this has been found the thrust of the PPT can be found.

In order to accurately measure the thrust from the PPT some sort of measurement must be taken when the thruster fires. Usually with a steady state thruster some sort of force transducer would be used to directly measure the thrust but with a pulsed firing thruster this cannot work because the pulses are usually much shorter than a second (on the order of micro seconds) and thus won't give any usable data.

Using Eq. 4 for the amplitude, we can rearrange it in terms of impulse bit and from there using impulse momentum theorem derive Eq. 7 below.

$$I_b = \frac{J\omega_n A}{l_{arm} l_{th}} = F\Delta t \qquad \text{Eq. 7}$$

This legacy method hinges on the ability to know what the natural frequency of the thrust stand is. As this method infer impulse from the excited oscillatory behavior of the fixture, it is less sensitive than it needs to be. In addition, the natural frequency of the fixture needs to be a well-defined function of impulse. In the case of this design (as will be discussed further in the Oscillatory Modes section and Thrust Stand Design sections) magnets center the arm and create the torsional stiffness. The issue with the magnets is that as two magnets approach each other (in both repulsion or attraction) the force changes as a function of distance squared meaning as the arm moves through an oscillation the spring constant will not be linear.

In this original work, a more sensitive instrument is built using a more direct approach. Instead impulse may be inferred directly as a momentum exchange between the

pendulum weight (for calibration) and the PPT. If the momentum of the torsional arm can be deduced as a function of the impulse of the thruster, the thrust may be inferred if the firing time can be recorded. Due to the implied rotation of the arm, the problem must be completed in terms of angular moment and not linear momentum.

We know the angular momentum can be defined as the moment of momentum around a center point governed by Eq. 8, where *L* is the angular momentum, *r* is the radius, *m* is the mass of the object, and *v* is the velocity of the object. Or conversely, the angular momentum is also equal to *I*, the mass moment-of-inertia of the object multiplied by the angular velocity of the object around the point.

$$L = \boldsymbol{r} \times m\boldsymbol{v} = I\omega \qquad \text{Eq. 8}$$

Once an impact has been imparted to the fixture, the velocity of the LVDT core can be calculated from the slope of the displacement curve initially after impact while it is still a relatively linear slope. The velocity of the core can then be converted into the angular velocity of the torsional arm (in rads/sec), Eq. 9 where *r* is the radius of the sensor core from the pivot point of the torsional arm.

$$\omega_{arm} = \frac{v_{LVDT}}{r_{LVDT}} \qquad \text{Eq. 9}$$

The next step is to plug in the calculated ω from Eq. 9, along with the radii and masses of the thruster and counterweight into Eq. 8, summed to gain the entire angular

momentum of the torsional arm. Once this has been completed, a unit check must be in order. The units of linear momentum and impulse in SI are N-s whereas angular momentum has units in SI of kg-m^2/sec. The units are not equal which makes sense, as the angular momentum is essentially the torque cause by linear momentum around a certain point. In order for this method to record impulse the angular momentum of the torsional arm must be divided by the radius at which the impulse is imparted on the torsional arm, in this case at l_{th}, the thrust line of the PPT, Eq. 10.

$$I_b = \frac{L_{stand}}{r_{th}} = \frac{\Sigma\, I\omega}{r_{th}} \qquad \text{Eq. 10}$$

The calibration of this method still falls along the same path as the previous method. Measured pendulum impacts at the thrust line on the arm and recording the resultant displacement curve. From this curve the velocity can be calculated from the initial linear displacement of the LVDT core immediately after impact. With a range of masses of pendulums, all dropped from the same height will produce a linear calibration line in which a calculated velocity from the displacement data will correspond to an impulse imparted into the arm.

The linear momentum of this pendulum, recalling Eq. 5, uses the mass of the weight multiplied by the velocity due to gravitational acceleration. To convert this into angular momentum, the linear momentum is multiplied by the radius of impact on the arm (the PPT thrust line, r_{th}) shown in Eq. 11.

$$L_{calibration} = P_{calibration} * r_{th} = m_{calibration} * \sqrt{2gh} * r_{th} \qquad \text{Eq. 11}$$

B. Static Balance & Mass Moments of Inertia

The next important set of dynamics to take into account is the static balance and mass moments of inertia of the fixture. Though the thrust stand is supposed to only move in a horizontal plane, it is important to look at all of these parameters: roll, yaw and pitch. As mentioned before, a knife edge bearing can move in all three directions. These calculations help to ensure the induced movement occurs solely in the yawing direction and not in the others.

For the mass moments of inertia, it important that our roll mass moment-of-inertia is much larger (at least a factor of ten larger) than the yaw mass moment-of-inertia. This requirement is derived from the fact that if the thrust vector of the PPT is not 100% horizontal the torsional arm will resist the bobbing motion in the pitch or roll and instead move in rotational (yaw) motion.

In order to meet static balance, Eq. 12 is used, which is turned into a ratio of masses to lengths for the thruster and counterweight.

$$m_{th} g l_{th} = m_{cw} g l_{cw} \quad \rightarrow \quad \frac{m_{th}}{m_{cw}} = \frac{l_{cw}}{l_{th}} \qquad \text{Eq. 12}$$

With the above ratios and knowing the mass of the thruster we can vary the mass of the counterweight and the length of the thruster arm in order to find the length of the counterweight arm. Now once these values have been calculated we can find the mass moment-of-inertia in yaw from Eq. 13.

$$I_{yaw} = \Sigma m r^2 = m_{th} l_{th}^2 + m_{cw} l_{cw}^2 \quad \text{Eq. 13}$$

Next the mass moment-of-inertia in roll needs to be calculated based on Eq. 14.

$$I_{roll} = I_{th} + m_{cw} l_{cw_z}^2 \quad \text{Eq. 14}$$

This equation moves the counterweight downward creating a pseudo pendulum with the counterweight in order to largely increase the rolling mass moment-of-inertia. The I_{th} term is the mass moment-of-inertia of the thruster itself because in this case the thruster cannot be assumed to be a point mass, so it is calculated by Eq. 15 where "*a*" and "*b*" are the footprint dimensions of the thruster.

$$I_{th} = \frac{1}{12} m_{th}(a^2 + b^2) \quad \text{Eq. 15}$$

Once the necessary mass moments of inertia were calculated varying the aforementioned parameters including the "*z*" arm length for the counterweight in *Excel* the roll to yaw mass moment-of-inertia ratios were calculated to find favorable dimensions for the thrust stand.

C. Oscillatory Modes

Not only do the mass moments of inertia matter, but additionally the oscillatory modes in each direction matter. There are two design constraints for this part: the first is that the rolling frequency mode shouldn't have values close to the yawing mode. This is decided upon to ensure that the torsional arm when excited in the yawing mode doesn't excite the other modes. The second constraint is the design of the yawing oscillatory period. As mentioned earlier in the paper the pulse is so small that the stand must accentuate the movement by designing the stand to have a time period of a few seconds in order to record the desired displacement data when the arm is excited by the thruster.

For the rolling mode, the equation of motion is:

$$\left(m_{cw}l_{cw,z}^2 + I_{th}\right)\ddot{\alpha} = -(m_{cw} + m_{th})g * sin(\alpha)l_{cw,z} \qquad \text{Eq. 16}$$

Using the small angle approximation and a forced solution of $\alpha = \sin(\omega t)\,\alpha_0$, the frequency mode is then solved to be Eq. 17.

$$\omega = \frac{1}{2\pi}\sqrt{\frac{(m_{cw}+m_{th})gl_{cw,z}}{m_{cw}l_{cw,z}^2+I_{th}}} \qquad \text{Eq. 17}$$

Plugging in all of the known values into Eq. 17, the rolling mode (in Hz) can be found where $l_{cw,z}$ is the length of the arm for the counterweight in the z-direction.

For the pitching mode of the thrust stand:

$$\left(m_{cw}(l_{cw,z}^2 + l_{cw}^2) + m_{th}l_{th}^2\right)\ddot{\gamma} = -m_{cw}g * sin(\gamma)l_{cw,z} \quad \text{Eq. 18}$$

Again, using the small angle approximation and a forced solution of $\gamma = \sin(\omega t)\,\gamma_0$, the frequency mode can be solved to be Eq. 19.

$$\omega = \frac{1}{2\pi}\sqrt{\frac{m_{cw}g l_{cw,z}}{m_{cw}(l_{cw,z}^2+l_{cw}^2)+m_{th}l_{th}^2}} \quad \text{Eq. 19}$$

With all of the known values the pitching mode can be found (in Hz), where l_{cw} is the length of the arm from the pivot to the counterweight horizontally, and l_{th} is the arm length from the pivot point to the thruster.

A large assumption that has been made throughout this design has been the angle approximation. In order to achieve this, the torsional arm must employ some sort of limit stays. In this case, the use of either a mechanical spring or a set of small permanent magnets used to restrict the movement of the arm and center it after being deflected. Running through similar frequency mode calculations, spring constants can be found for the centering springs by setting a desired frequency. Unfortunately, the spring constants for a frequency of 0.3 Hz or a time period of approximately 3 seconds per full oscillation would require springs with a spring rate on the order of 10^{-5} lbs/in, which is impractical to procure.

Because the required spring rate is so low, coil springs cannot be considered for instrument centering. Instead, a set of small magnets can initially center the arm and provide some spring effect needed to ensure very slow undamped periodic motion. Due to the non-linear nature of a magnets attractive/repulsive force, a series of magnets were tested at different distances from the centered arm to in an attempt to develop an empirical database of magnets and spacing in order to design to a certain frequency response. The magnets must be small enough that the magnetic field of the magnets will be weak enough that they will not affect the electromagnetic field of the thruster.

D. Thrust Stand Data Measurements

The LVDT, when the core is moved, gives an output voltage signal. This voltage signal is sent through an analog signal processor (in this fixture, an AD598 analog chip) which outputs a linear voltage signal which the computer records via data acquisition hardware and LabVIEW. The LabVIEW Virtual Instrument (VI) takes the voltage signal and transforms it into plottable displacement data. This displacement data will then be input into an Excel document. The initial, displacement can be fit with a linear equation to get its slope (this corresponds to the velocity of the LVDT core). It is important to note that a conversion from volts to meters (or inches) will be required to convert from the voltage reading from the LVDT and the Data Acquisition hardware (DAQ) into a position and consequently velocity measurement.

IV. THRUST STAND DESIGN

A. Preliminary Design

The thruster that will be tested here was designed and built by Sun Devil Satellite Laboratory, a student organization at Arizona State University. The footprint dimensions of the PPT are 0.1m by 0.1m; it has a mass of about 300 grams. The thruster is estimated to have an impulse bit of about 275 μN-s with an estimated pulse time of about 9 μs.

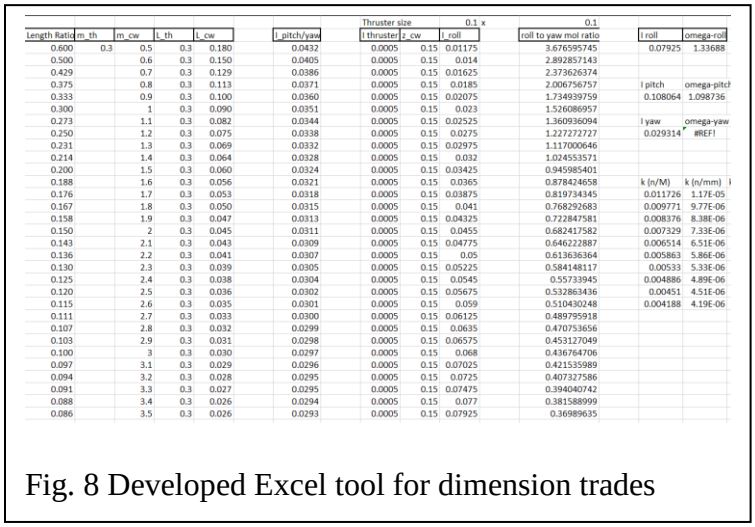

						Thruster size		0.1 x	0.1		
Length Ratio	m_th	m_cw	L_th	L_cw	I_pitch/yaw	I thruster	z_cw	I_roll	roll to yaw mol ratio	I roll	omega-roll
0.600	0.3	0.5	0.3	0.180	0.0432	0.0005	0.15	0.01175	3.676595745	0.07925	1.33688
0.500		0.6	0.3	0.150	0.0405	0.0005	0.15	0.014	2.892857143		
0.429		0.7	0.3	0.129	0.0386	0.0005	0.15	0.01625	2.373626374		
0.375		0.8	0.3	0.113	0.0371	0.0005	0.15	0.0185	2.006756757	I pitch	omega-pitch
0.333		0.9	0.3	0.100	0.0360	0.0005	0.15	0.02075	1.734939759	0.108064	1.098736
0.300		1	0.3	0.090	0.0351	0.0005	0.15	0.023	1.526086957		
0.273		1.1	0.3	0.082	0.0344	0.0005	0.15	0.02525	1.360936094	I yaw	omega-yaw
0.250		1.2	0.3	0.075	0.0338	0.0005	0.15	0.0275	1.227272727	0.029314	#REF!
0.231		1.3	0.3	0.069	0.0332	0.0005	0.15	0.02975	1.117000646		
0.214		1.4	0.3	0.064	0.0328	0.0005	0.15	0.032	1.024553571		
0.200		1.5	0.3	0.060	0.0324	0.0005	0.15	0.03425	0.945985401		
0.188		1.6	0.3	0.056	0.0321	0.0005	0.15	0.0365	0.878424658	k (n/M)	k (n/mm)
0.176		1.7	0.3	0.053	0.0318	0.0005	0.15	0.03875	0.819734345	0.011726	1.17E-05
0.167		1.8	0.3	0.050	0.0315	0.0005	0.15	0.041	0.768292683	0.009771	9.77E-06
0.158		1.9	0.3	0.047	0.0313	0.0005	0.15	0.04325	0.722847581	0.008376	8.38E-06
0.150		2	0.3	0.045	0.0311	0.0005	0.15	0.0455	0.682417582	0.007329	7.33E-06
0.143		2.1	0.3	0.043	0.0309	0.0005	0.15	0.04775	0.646222887	0.006514	6.51E-06
0.136		2.2	0.3	0.041	0.0307	0.0005	0.15	0.05	0.613636364	0.005863	5.86E-06
0.130		2.3	0.3	0.039	0.0305	0.0005	0.15	0.05225	0.584148117	0.00533	5.33E-06
0.125		2.4	0.3	0.038	0.0304	0.0005	0.15	0.0545	0.55733945	0.004886	4.89E-06
0.120		2.5	0.3	0.036	0.0302	0.0005	0.15	0.05675	0.532863436	0.00451	4.51E-06
0.115		2.6	0.3	0.035	0.0301	0.0005	0.15	0.059	0.510430248	0.004188	4.19E-06
0.111		2.7	0.3	0.033	0.0300	0.0005	0.15	0.06125	0.489795918		
0.107		2.8	0.3	0.032	0.0299	0.0005	0.15	0.0635	0.470753656		
0.103		2.9	0.3	0.031	0.0298	0.0005	0.15	0.06575	0.453127049		
0.100		3	0.3	0.030	0.0297	0.0005	0.15	0.068	0.436764706		
0.097		3.1	0.3	0.029	0.0296	0.0005	0.15	0.07025	0.421535989		
0.094		3.2	0.3	0.028	0.0295	0.0005	0.15	0.0725	0.407327586		
0.091		3.3	0.3	0.027	0.0295	0.0005	0.15	0.07475	0.394040742		
0.088		3.4	0.3	0.026	0.0294	0.0005	0.15	0.077	0.381588999		
0.086		3.5	0.3	0.026	0.0293	0.0005	0.15	0.07925	0.36989635		

Fig. 8 Developed Excel tool for dimension trades

As mentioned in the Thrust Stand Dynamics section, the static balance, mass moments of inertia and the frequency modes drive the dimensions of the torsional arms and the mass and location of the counterweight. A tool was created in *Excel* in order to run trade studies on the needed dimensions (see Fig. 8).

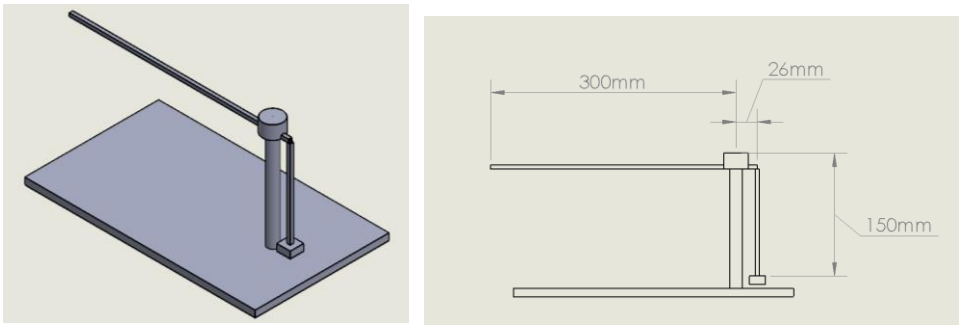

Fig. 9 Preliminary CAD drawing of thrust stand

On the left side, there are columns for the length ratio, mass of the thruster (known), mass of the counterweight, length of the arm to the thruster and horizontal length of the arm to the counterweight. The mass of the counterweight is varied as well as the length of the thruster arm length to get the other values. The mass moment-of-inertia for yaw is calculated from the lumped mass and parallel axis theorem. The mass moment-of-inertia of the thruster is calculated and the vertical length of the counterweight arm is varied, this leads to a ratio of rolling mass moment-of-inertia to yawing mass moment-of-inertia. This value is desired to be less than 1, closer to 0 the better because if there is any misalignment the torsional arm will want to move in the yawing direction more than roll.

This possible design gives a static balance, as well as meets the set criteria for the mass moments of inertia ratios. Fig. 9 shows a preliminary design in CAD with dimensions shown using the values from Table 1 for the thrust stand.

Not shown in Fig. 9 is the placement of the centering magnets. The magnets will be smaller than 10 mm in diameter and no thicker than 5 mm. In the *Excel* tool the placement

of “springs” is varied along the torsional arm (no further than half way along the arm) to find a range of spring constants to re-center the arm.

Using this and information about the magnets repulsive force as a function of distance the spring constants can be found for the magnets as a function of distance and suitable magnets to center the arm after it has been deflected by the thruster.

Table 1 – Preliminary Thrust Stand Design Dimensions

m_{th}	m_{cw}	l_{th}	l_{cw}	$l_{cw,z}$
0.3 kg	3.5 kg	0.3 m	0.026 m	0.15 m
I_{pitch}	I_{yaw}	I_{th}	I_{roll}	I_{yaw}/I_{roll}
0.0293 kg-m^2	0.0293 kg-m^2	0.0005 kg-m^2	0.07925 kg-m^2	0.3698

B. Detailed Design

Once construction started on the fixture, small changes and adjustments were made to the preliminary design described earlier. Some of the changes made include adjusting the mass of the thruster simulate, counterweight, and arm lengths. The changes made were not drastic and left the thrust stands characteristics similar to that of the preliminary.

In order to get the moments of inertia as low as possible without sacrificing other desired characteristics the 300 gram thruster was reduced to 100 grams. The original estimated 300 grams was for an array of 4 thrusters, the new estimate is for a single thruster and some “crud” weight for a nice even number.

Additionally, the arm lengths we adjusted from the preliminary design, keeping static balance and similar mass moment-of-inertia ratios. This was done in order to decrease the overall mass of the counterweight due to the sheer size of material needed to be sufficient. The length ratio was brought to a 10:1 ratio, meaning the thruster arm was 10 times the length of the counterweight horizontal arm while the mass of the counterweight was 10 times that of the thruster. This ratio is the "perfect" condition, in reality the attachment for the PPT added some weight and the LVDT core attachment did as well so the counterweight is not a 10:1 ratio. The vertical height of the counterweight was adjusted to bring the moment-of-inertia ratios closer to the more favorable ratios of the preliminary design. As Table 1 (previous page) and Table 2 can be compared, the ratios of the preliminary design and the final design are very close to each other while using lighter masses and longer arms. Other configurations with a similar ratio are possible, this is the design chosen for this experiment.

Table 2 –Final Thrust Stand Design Dimensions

m_{th} (with attachment)	m_{cw}	l_{th}	l_{cw}	$l_{cw,z}$
0.156 kg	2.04 kg	0.4 m	0.04 m	0.2 m
I_{pitch}	I_{yaw}	I_{th}	I_{roll}	I_{yaw} /I_{roll}
0.0282 kg-m^2	0.0282 kg-m^2	0.00026 kg-m^2	0.08186 kg-m^2	0.344

After of the constraints and issues were resolved, the stand was built as described in the Construction section. Table 2 shows the final dimensions and estimated mass moments of inertia. The final design built test stand can be seen in Fig. 10.

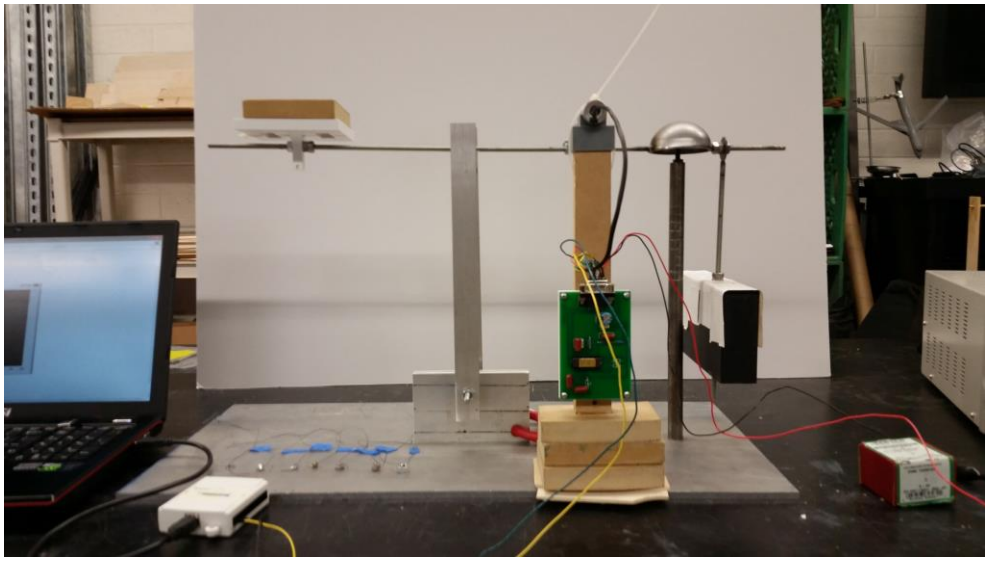

Fig. 10 Final test stand setup

The thrust stand performed well within the range of expected impulse simulated by a pendulum. As will be seen later in the data section (Section V, Part C) the thrust stand was capable of measuring 330 μN-s with a reasonable level of accuracy. The data gets less noisy and is easier to record for the larger impulses. No attempts were made to go below the target impulse for fear of data clarity due to the noise in the sensor. Later in the error analysis section the noise is characterized and an estimation tool is implemented. Theoretically the fixture is capable of measuring half of the target impulse before noise overwhelms the input. If a more precise LVDT with less signal noise were to be used, this thrust stand could very well be capable of recording even smaller impulses. For the

moment, the thrust stand meets the target impulse with a reasonable amount of error in the values (approximately within 10% of expected values).

C. Construction

Based upon the preliminary design dimensions the construction of the test stand was planned to be done using precisely machined parts with the assistance of the student machine shop located at the ASU-Tempe campus. Due to scheduling conflicts, the construction was shifted to a simpler, less refined method that could be completed in the remaining time and budget.

The pivot cup was originally to be machined out of a solid piece of steel round bar with holes to fasten the thruster arm and counterweight arms to the cup. The new design uses a prefabricated hollow hemisphere purchased over the internet. The hollow hemisphere holds the same diameter dimension of 2.5 inch (~0.635 m) as the machined piece, but in the end, the new cup is lighter and doesn't require the need for machining it.

The thruster and counterweight arms were to be made from steel thin walled tubing with attachment points for the PPT/LVDT and counterweight. The new design uses ¼ inch (0.00635 m) all-thread rod for the arms, which are welded onto the cup in the appropriate places. The vertical counterweight arm is also ¼ inch (0.00635 m) all-thread rod with a washer welded to one end for attachment to the horizontal arm on the pivot cup. The use of all-thread rod allows the user of the thrust stand to adjust the position of the thruster attachment, the horizontal position of the counterweight, and the vertical placement of the

counterweight. All of the attachments are done using two hex nuts on each side of the component to lock it in place but keep it easily adjustable. This adjustability is useful if the user plans on updating components of the thrust stand, or wants to adjust the static balance/dynamic properties of the test stand. In the case of this experiment the adjustability of the weight was used to overcome small inconsistences in the calculated model and the constructed stand.

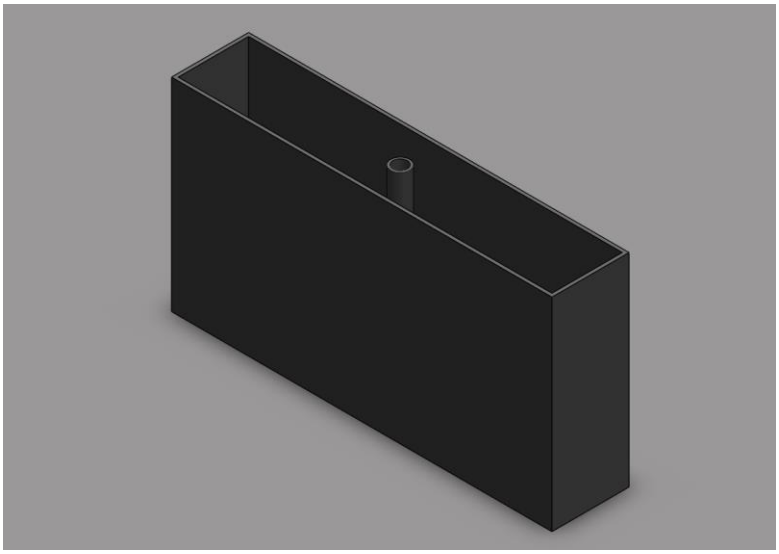

Fig. 11 Counterweight cup rendered in Solidworks

The counterweight consists of two components, the "counterweight cup" and the material used for the weight. Currently the counterweight cup was design in Solidworks and 3-D printed out of polylactic acid (PLA) and dimensioned to the correct inner volume of material needed to be a sufficient counterweight. The material used as the weight was chosen to be lead shot due to its relatively high density. This causes the volume of material

for the weight to be smaller and easier to handle. Fig. 11 is the counterweight cup rendered in Solidworks and Fig. 12 shows the counterweight cup filled and attached to the test stand.

Fig. 12 Counterweight cup attached to vertical counterweight arm

Fig. 13 Torsional arm pivot point attachment

The base of the test stand is simply a plate of aluminum with holes drilled and countersunk into it in the required positions for the attachment of the pivot point bar. The pivot point bar is a ½ inch (0.0127 m) diameter piece of steel bar with threaded holes on each end, one for attachment to the base plate and the other for a prefabricated point with threads on it. Fig. 13 (previous page) exhibits the pivot point attached to the base plate for the test stand.

The PPT attaches to the pivot arm via another 3-D printed PLA part deigned in Solidworks, using the footprint dimensions and the placement of the screw holes of the PPT. The PPT attachment plate slides onto the all-thread rod and is clamped into place by two sets of hex nuts tightened on each side as mentioned before, Fig. 14.

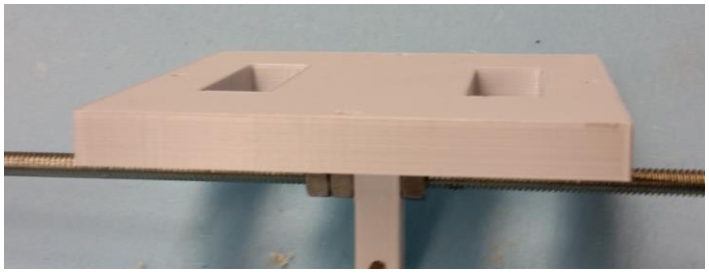

Fig. 14 3-D printed PPT attachment

The LVDT comprises the main sensor body and the sliding core. The sliding core is attached to the arm of the test stand while the main sensor body is attached to the base of the stand in order to hold it in place. On the original design the sliding core piece was attached at the point the PPT was attached to get the exact displacement. Due to the small perturbations in the thruster arm the LVDT's core was shifted closer to the pivot point and

shifted upwards to be in line with the horizontal plane of the pivot point to reduce the unwanted movement. While the angular displacement is within the small angle approximation the LVDT core would in some cases bind with the main body. To fix this problem a small all-thread rod end with a ball joint was attached to the core rod to keep the core moving in a linear motion, all attached to a 3-D printed piece seen in Fig 15.

Fig. 15 3-D printed LVDT main body and core attachment with ball joint

Additionally, the LVDT was replaced by one with a larger tolerance between the outer radius of the core and the inner radius of the main body. A comparison of the first LVDT used and the replacement LVDT with larger hole tolerance is shown in Fig. 16 (overleaf).

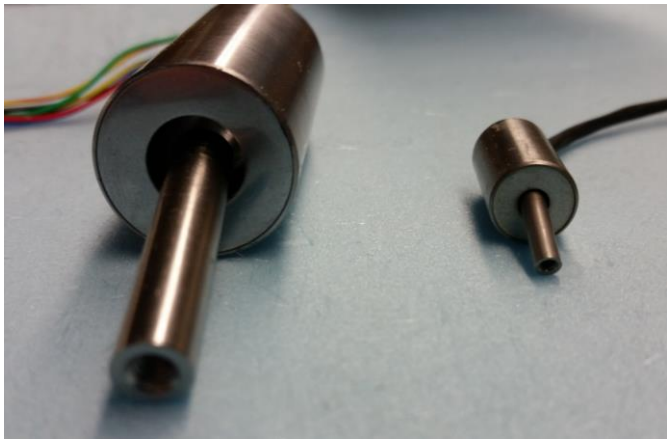

Fig. 16 Comparison of LVDT core to main body hole tolerance

The main body of the LVDT and the signal conditioner board attaches to a small stand. This places the LVDT main body at the same height as the sliding core on the thruster arm. This LVDT stand is made out of Medium-density fiberboard (MDF) and two 3-D printed PLA pieces. One piece is attached to the top of the stand and has a half cylinder slot of the LVDT main body to sit in by a friction fit, this piece was redesigned to accommodate the new LVDT after the binding issues were discovered and to ensure the LVDT doesn't move, it is secured by a zip-tie, Fig. 17 (overleaf). The second piece is a bracket to hold the signal conditioner on the side of the stand due to the short wire runs from the LVDT to the conditioner, Fig 18 (overleaf). The wires from the conditioner go to the DAQ and into the computer.

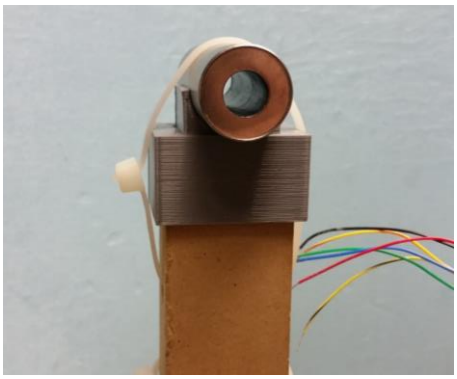

Fig. 17 LVDT and 3-D printed attachment piece

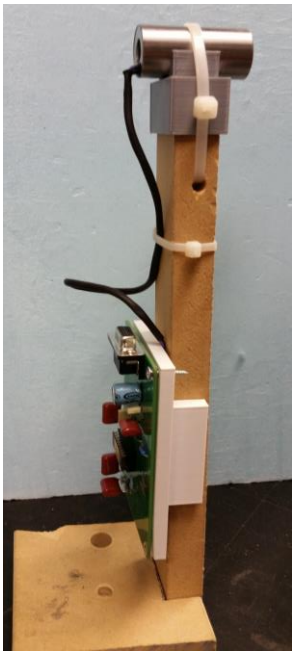

Fig. 18 LVDT stand with 3-D printed parts

The magnets on the thruster arm are attached to a hex nut to allow for easy adjusting of placement and hence centering. The second set of magnets are attached to small aluminum

bars on a small piece of all-thread rod to allow for distance adjustment of the repulsive force of the magnets. Unfortunately, the data available on the magnets purchased for the test stand did not have high enough resolution of the magnet to magnet repulsion force at specified distances. The magnets were calibrated using a simulated pendulum impact. Due to the non-linearity of the magnetic repulsion, there is not a constant oscillatory frequency of the torsional arm. Thus, the sizing of the magnets must be on a case by case basis. The larger the impulse to be recorded, it must be assured that the impulse won't fully displace the arm and cause the magnets to jump and attach to each other.

In the case of this setup, Neodymium magnets that are ¼ inch (0.00635 m) wide and 1/32 inch (~0.0008 m) thick proved effective. The outside set were placed a distance of about 1.325 inch (0.0336 m) on either side of the arm, Fig 19. This placement allowed for the largest and smallest calibration weight to not be impeded by the repulsive force but enough to center the arm and control the maximum deflection.

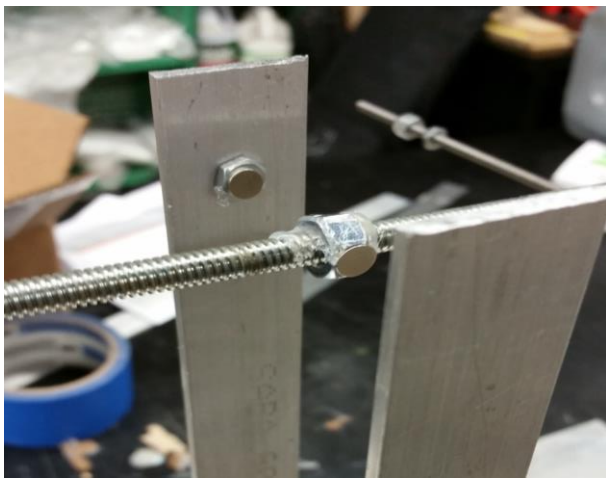

Fig. 19 Magnets centering the torsional arm

V. EXPERIMENTAL TEST

A. Calibration Test

In order to calibrate the thrust stand, its response to known impulses must be characterized. To develop these impulses, a known mass at a known velocity tangentially impacts the torsional arm at the thrust line. As previously mentioned in Eq. 11, a selection of test weights released from calculated heights accurately impart an impulse. Due to the impulse momentum approach of the analysis, the pendulum impacts were as close to in-elastic as possible (Fig. 20).

$$L_{calibration} = P_{calibration} * r_{th} = m_{calibration} * \sqrt{2gh} * r_{th} \qquad \text{Eq. 11}$$

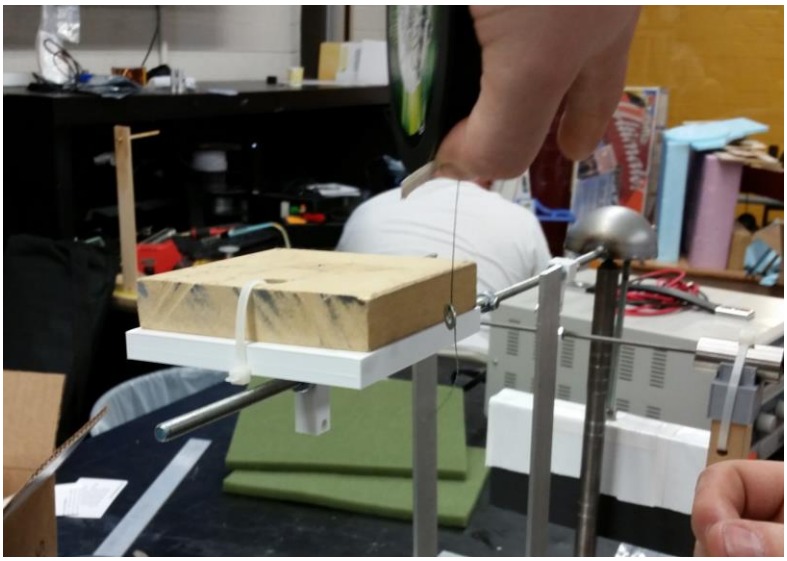

Fig. 20 In progress pendulum testing

All pendulums used were small nuts and washers all weighed using a precision scale ranging from the target mass up to approximately 10 times the mass. The masses of the pendulums are listed in Table 3. The height at which the pendulums were dropped was calculated to be 5 cm in order to be as close to the target impulse as possible. Each pendulum was dropped from the same height in order to keep the change of impulse to be purely based upon the mass of the pendulum. The pendulums used can be seen in Fig. 21, the blue tape on the string indicates the prescribed height at which to hold to string to ensure the 5 cm drop height.

Table 3 – Test pendulum info

	Mass (gram)	Height (cm)	Impulse (N-s)
Pendulum 1	0.3	5	0.000297
Pendulum 2	0.6	5	0.000594
Pendulum 3	0.9	5	0.000891
Pendulum 4	1.0	5	0.00099
Pendulum 5	1.2	5	0.001189
Pendulum 6	1.8	5	0.001783
Pendulum 7	3.3	5	0.003268

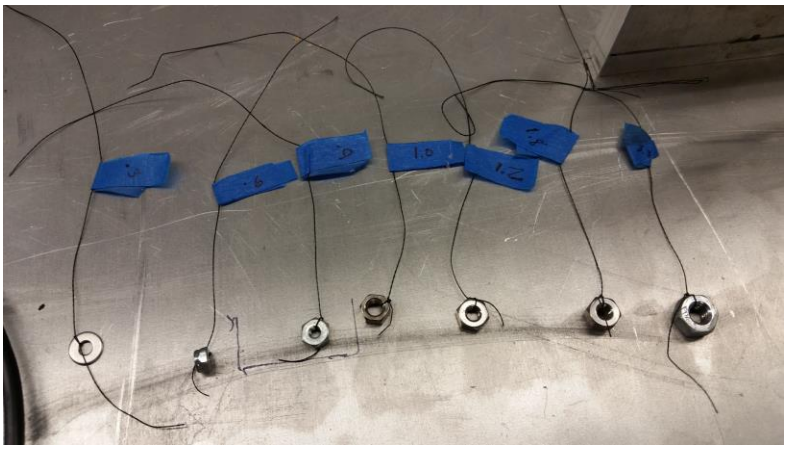

Fig. 21 Pendulums used in testing

To calibrate the magnets, the process was somewhat trial and error. Starting with the smallest set of magnets placed 2 inch (0.0508 m) away from the torsional arm. A pendulum simulating approximately 3.25e-3 N-s of impulse impacts the torsional arm. Once impacted, the torsional arm moves and its position data is recorded by LabVIEW. The data was then processed in order to calculate the frequency of oscillation. The first test produced a frequency lower than the desired frequency of 0.3 Hz, thus the magnets were shifted inwards, closer to the arm and retested.

This process was repeated, adjusting the magnets inwards and outwards until the desired frequency was achieved as closely as possible, using both the high and low end impulse values. This frequency does not need to be exact due to the nature of the impulse momentum approach, it is purely meant to ensure that the torsional arm won't over extend for the high impulse case and will still would have enough of an oscillatory motion for the DAQ to record the data.

The last bit of calibration that was required was to experimentally calculate the conversion factor from volts to inches and then into meters on the LVDT. Initially the conversion factor used was 0.01 V/in, this comes from a voltage of +/- 10 V and a stroke of +/- 0.1 in. In order to verify this conversion a small setup was made. The setup for this calibration was relatively simple. The LVDT core piece is threaded onto additional rod, which had two hex nuts on the other end. One of the nuts was glued into place on the rod to ensure it would not move during the test. The second was glued to the table to ensure

the entire setup could not move. The LVDT main body was placed so the core was mostly centered on the core.

The distance between the two nuts was measured initially with calipers to be 1.831 inch (0.0435 m). While the DAQ was recording the displacement in voltage the rod was slowly turned pushing the core further into the LVDT. Once completed the new distance between the nuts was measured to be 1.7435 inch (0.04428 m) and the difference in the voltage recorded by the LVDT was found to be 7.067 V. The distance was then divided by the change of voltage recorded by the LVDT and DAQ to get the new V/in calibration. The final experimental conversion was found to be 0.012381 V/in or 0.0003144 V/m. The raw LVDT data can be found in Appendix B.

B. Raw Data

LabVIEW was used to record the data from the LVDT and DAQ. This required a VI (user interface) to be constructed within LabVIEW to visualize the real-time data and to save it into a file which would be used to calculate the necessary values to find the impulse. After much trial and error, a VI and accompanying block diagram was created. As can be seen in Fig. 22 (overleaf), the VI is as simple as possible. The waveform graph will show the output of the LVDT displacement in real-time. The amplitude and frequency boxes will display the relevant data output as calculated by LabVIEW through a signal processing block. Finally, the most important feature is the save button. Once the test stand is ready to record data the user will press that button and LabVIEW will begin recording data into a

text file which will later be input into *Excel* for post-processing, to stop recording the button must be pressed again.

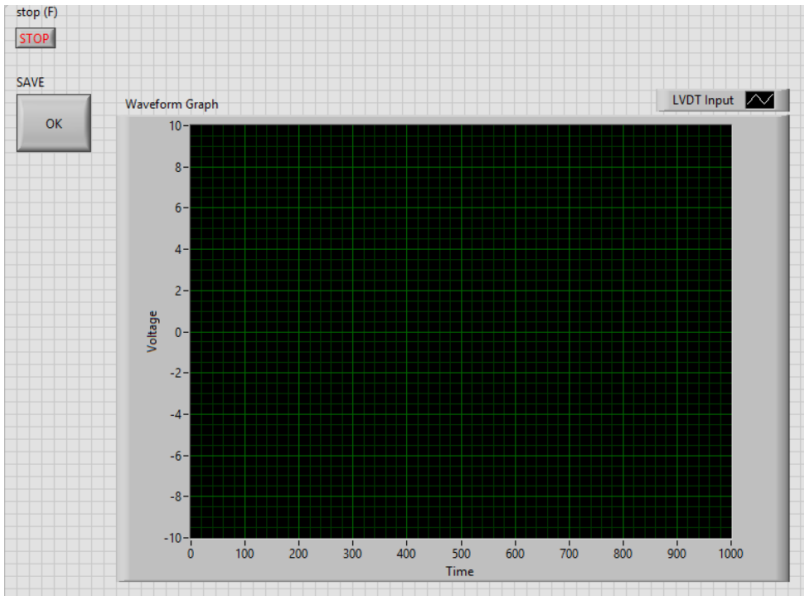

Fig. 22 LabVIEW VI user interface

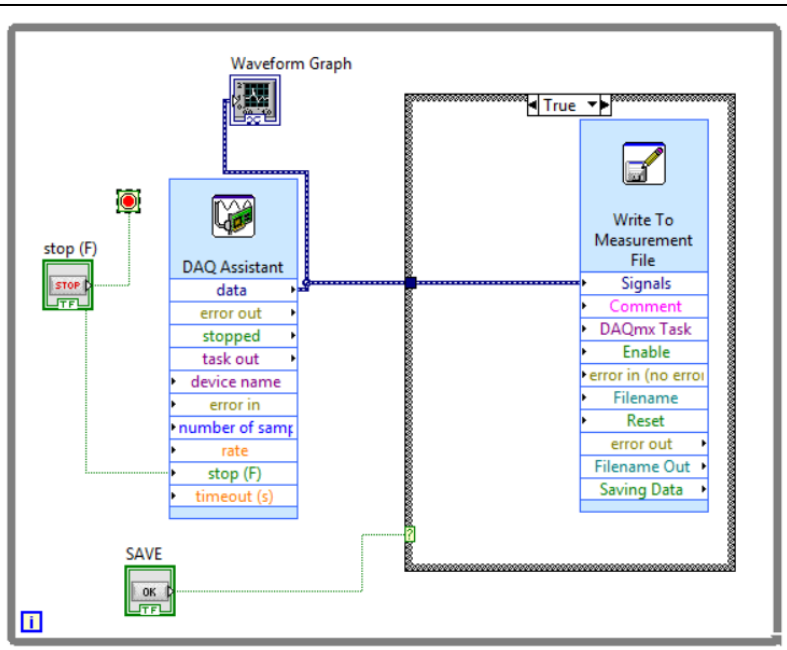

Fig. 23 LabVIEW VI block diagram for LVDT data recording

The block diagram is the behind the scenes framework for the VI. The block diagram seen in Fig 23 (previous page) is the setup for the recording VI for the LVDT. The DAQ Assistant block is how LabVIEW reads the voltage data from the DAQ and also controls the sample buffer and the rate at which data recorded. In this case the data was sampled at a rate of 250 Hz or 1 sample every 0.004 seconds. The voltage data is fed into the waveform graph block which displays it to the user on the VI. This voltage is also piped into a Write Measurements block. In the block's options the user can decide the file formatting of the data file. Fig. 24 (overleaf) displays a sample voltage "displacement" plot where a 0.9 gram weight was used to create the impulse. A reading of +/-10 volts represents the full core stroke position of the LVDT, which is the maximum possible voltage recordable by the DAQ.

In order to ensure any one pendulum impact was good or bad up to 12 impacts were made with each pendulum so any "bad" impacts could be removed from the data set as not to skew the results of the tests. A possible reason for a bad impact would be impacting the PLA attachment for the PPT and not the MDF which better transferred the impulse or the pendulum had a bad impact and did not transfer all of its momentum into the thrust stand.

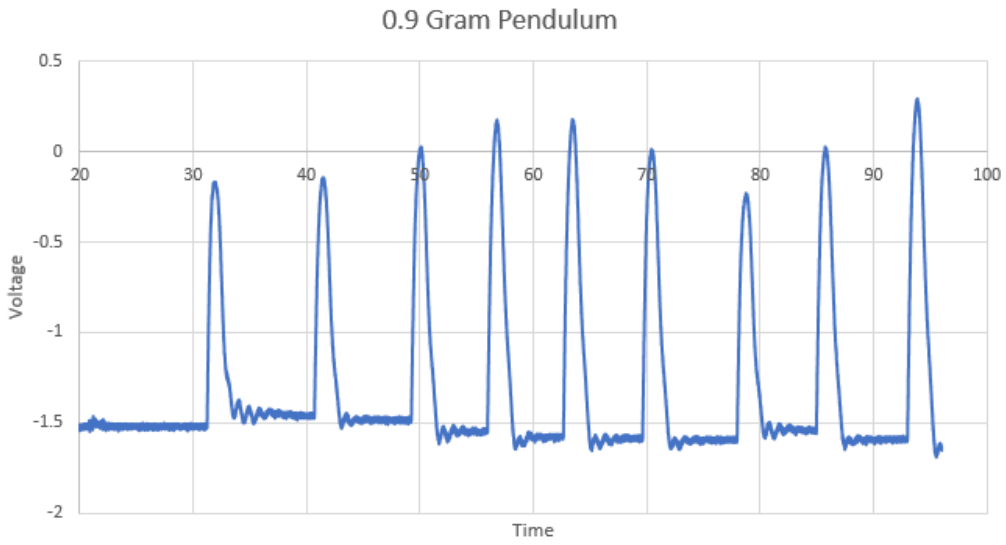

Fig. 24 Sample LVDT displacement waveform plot showing multiple impacts

Additional raw data and impact plots similar to the example can be found in Appendix A of this paper.

C. Post-Processed Data

Once the data has been recorded through LabVIEW, the data file is taken and imported into *Excel*. Each data file consists of multiple pendulum impacts and thus each impact must be separated in order to get the velocity of the LVDT core. This is done by plotting the entire data set and zooming in on the linear sections of each impact. Once zoomed in the time window of data is written down and a new plot is created of just the data in the time window, Fig. 25 (overleaf).

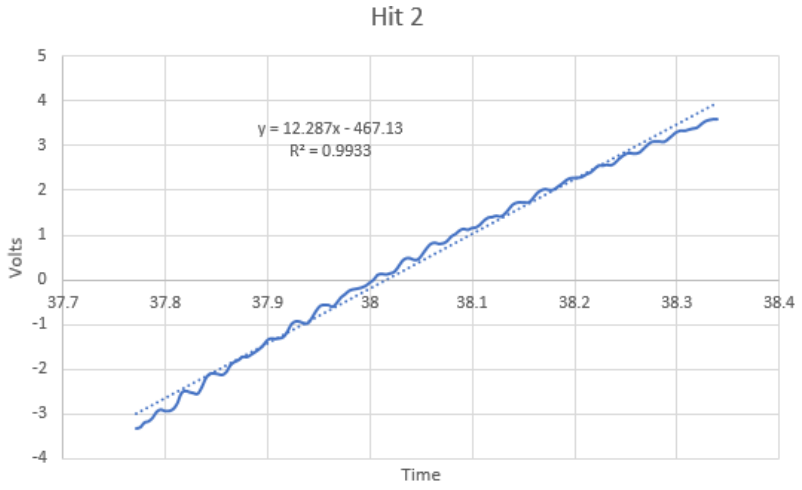

Fig. 25 Initial impact position data and velocity trendline

A linear trendline is then fit to the data and the corresponding R^2 values is displayed as well to indicate how "well" the trendline matches with the data, a value of 1.0 is the best. The process of finding the velocity via the trendline method is repeated for all 7 pendulums and all impacts made by each one.

For this experiment to be more accurate and repeatable the number of impacts should be increased up to at least 30 samples of each pendulum should be taken in order to represent a normal distribution of a data set. Because the data used here does not exceed 30, it falls under Student's T-distribution which does not cover a normal distribution. The closer to 30 samples, the closer it represents the normal distribution. Additionally, since the sample sets are below 30 the confidence interval of the data is larger than that of one with at least 30 data points. This is because as you approach 30 samples the data becomes less skewed due to outliers in the sets.

Once all of the velocities were found the average of all of the velocities were taken as well as the standard deviation in order to get a sense of the overall error across all of the data sets. All of the percent errors (standard deviation divided by the average) were under 10% which was deemed acceptable for this experiment, as seen in Fig. 26.

3.3 gram				1.8 gram				1.2 gram				1.0 gram			
V/sec	mean	Std Dev	% err	V/sec	mean	Std Dev	% err	V/sec	mean	Std Dev	% err	V/sec	mean	Std Dev	% err
11.211	11.5704	1.00916	8.72186	7.1768	7.0646	0.33403	4.72818	4.307	4.54516	0.22303	4.90699	3.6	4.07706	0.40215	9.86385
10.519				7.3613				4.3812				4.2252			
10.001				7.1343				4.7206				4.1717			
12.389				6.3576				4.4405				4.7892			
11.989				7.0156				4.2882				4.0373			
12.287				7.3111				4.582				3.6265			
12.597				7.0955				4.7796				4.0895			
								4.8622							

0.9 gram				0.6 gram				0.3 gram			
V/sec	mean	Std Dev	% err	V/sec	mean	Std Dev	% err	V/sec	mean	Std Dev	% err
3.8385	3.5815	0.20491	5.72129	2.6015	2.72247	0.2064	7.58123	1.2182	1.33018	0.11302	8.49684
3.3681				2.8236				1.3694			
3.5218				2.496				1.213			
3.7283				2.9313				1.272			
3.696				2.5261				1.4235			
3.3363				2.9563				1.485			

Fig. 26 Mean, standard deviation and percent error of recorded data

With the data in an acceptable range the next step is to convert the V/sec velocities into actual velocity of in/sec and finally into m/s. This is completed using the conversion factor mentioned earlier of 0.012381 V/in and also the conversion of 0.0254 m/in which gives 0.0003144 V/m. With the data into velocities of m/s the next step was to convert into angular velocity of rad/s by dividing the velocities at the LVDT by the radius at which it sits from the pivot point.

Using the angular velocity of the torsional arm, the angular momentum of the stand after impact was inferred using the masses of the counterweight/cup and MDF/attachment as

well as the corresponding radii. The angular momentums of the counterweight/cup and MDT/attachment were added together due to both rotating in the same direction. This angular momentum was then compared to the expected angular momentum imparted into the torsional arm by the pendulum impacting at the thrust line by creating a ratio of actual divided by expected. All of the test cases, except the 0.3 gram case and 0.6 gram case, were within 6% of the expected value. The 0.3 gram case and 0.6 gram case were within 11% and 16% respectively, these results will be further analyzed in the Discussion section. The final velocities and angular momentums can be seen in Table 4 and Table 5.

Table 4 – Table of calculated velocities at LVDT

m (kg)	v (in/sec)	v (m/sec)	ω (rad/s)
3.3	0.14326	0.00364	0.04548
1.8	0.08747	0.00222	0.02777
1.2	0.05572	0.00142	0.01769
1.0	0.05048	0.00128	0.01603
0.9	0.04434	0.00113	0.01408
0.6	0.03371	0.00086	0.0107
0.3	0.01647	0.00042	0.00523

Table 5 – Calculated and expected momentum with ratios

$L_{expected}$	$L_{thruster}$	L_{cw}	L_{total}	L ratio
0.0013074	0.00114	0.00017	0.0013041	0.99748
0.0007131	0.00069	6.3E-05	0.0007561	1.06028
0.0004754	0.00044	2.6E-05	0.0004671	0.98243
0.0003962	0.0004	2.1E-05	0.0004210	1.06265
0.0003566	0.00035	1.6E-05	0.0003676	1.03094
0.0002377	0.00027	9.3E-06	0.0002765	1.16309
0.0001189	0.00013	2.2E-06	0.0001327	1.11691

The final step was to take the velocity recorded by the LVDT and plot it against the experimental impulse of the pendulums. To get the impulse all that needs to be done is to divide the angular momentum L_{tot} by the radius from the thrust line to the pivot point which is 0.4 m. Table 6 gives the velocities and resulting impulse of each pendulum.

Table 6 – LVDT velocities and thrust stand impulse

v (m/s)	I_b (N-s)
0.00364	0.00326
0.00222	0.00189
0.00142	0.00117
0.00128	0.00105
0.00113	0.00092
0.00086	0.00069
0.00042	0.000332

These values are plotted, velocity on the *x-axis* and impulse on the *y-axis*, a linear fit line can be created which will allow the conversion of velocity read by the LVDT into the equivalent impulse of the impact. The resulting conversion equation from the fit line is Eq. 20, it can see in Fig. 27 (overleaf) the plotted data and trendline, calculated using significant figures tracked through *Excel*.

$$I_b = 0.882 * v_{LVDT} \qquad \text{Eq. 20}$$

You can see that the trendline and data shows a linear relationship between velocity measured by the LVDT and the impulse of the impact. Using Eq. 20, the impulse of the

PPT or pendulums is calculated based upon the linear velocity of the torsional arm caused by the PPT. Additionally, in Fig. 27 the scatter points for the pendulum cases were plotted to show their relation and give an idea of the confidence of the data. Most of the points clump together which is to be expected but there are some outliers. If, as mentioned before, the sample size was increased to at least 30 the clumping would persist with some outliers but the confidence of the data would get better as the samples increased because there is less of an effect by the outlying data.

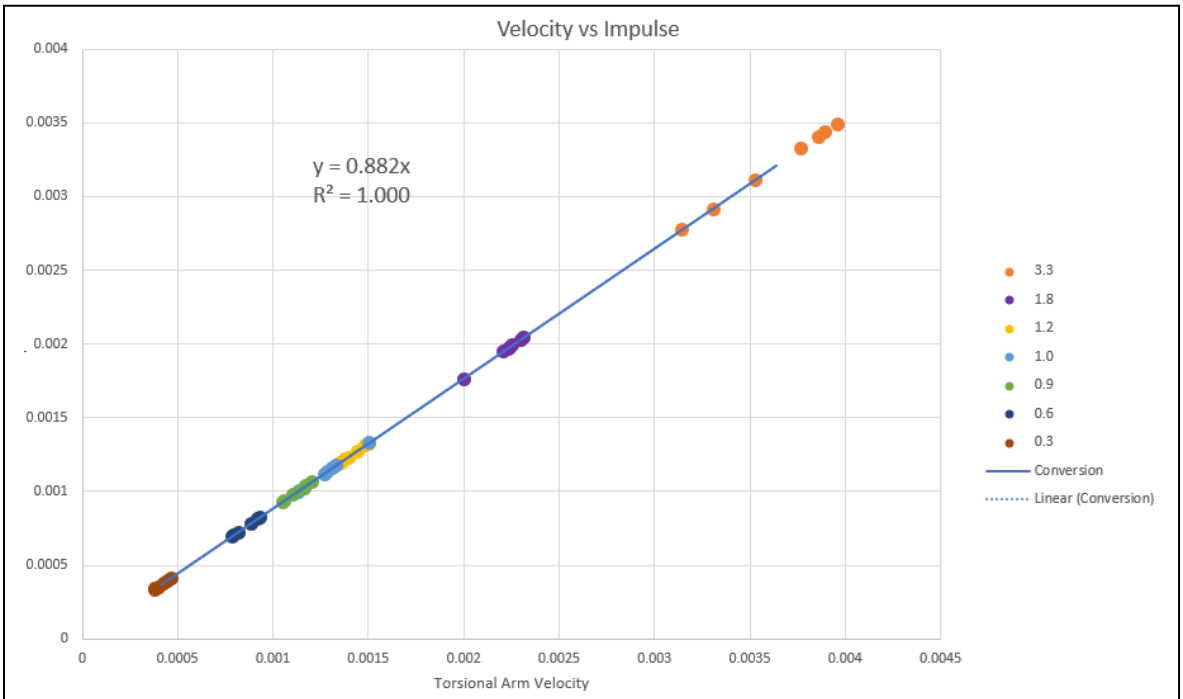

Fig. 27 Plotted velocity and impulse with trendline & scatter points to show confidence

D. Error Analysis

After the test data is processed and the impulse is calculated it is important to look at the error sources inherent in the data reduction process. The largest contributor to error can be assumed to be the noise of the sensor/signal conditioner. Others may include, small variations in the point of impact, small variations in the pendulum height, and finally the measured mass of the pendulums.

The "noise" of the sensor is by far the largest contributor to the error in impulse compared to the measured values. The noise of the sensor can be characterized by a uniform random "hiss". In order to measure this "hiss", multiple measurements were taken where the LVDT core did not move. In theory this should produce constant voltage a reading; in reality the digitized signal fluctuates over a range of voltage. The standard deviation of the straight lines of data is calculated and converted into meters. This value is taken as the noise on any measurement of displacement in meters and will henceforth be just called the ambient noise.

The next step in the noise analysis takes the conversion fit line for impulse to velocity and couples it with the ambient noise. Impulses, including those tested in the experiment were plugged back into the fit line to get their corresponding velocities. This velocity is then multiplied by a range of time values to get expected "noiseless" displacement points which are plotted. Now, the ambient noise must be added using a random number function multiplied by the ambient noise value. It is set up to add noise on either side of a data point

to simulate the noise in the actual sensor/conditioner. The new noisy data was fit with a linear trendline and the slope (velocity) of the noisy data is recorded.

Multiple slopes of the noisy data are recorded for a range of impulses (including those used in the experiment). The standard deviation and mean of these velocities is calculated and the deviation is divided by the mean to get the percent error of each expected velocity. The impulse and percent error were then plotted to show how the error changes as a function of impulse, see Fig. 28.

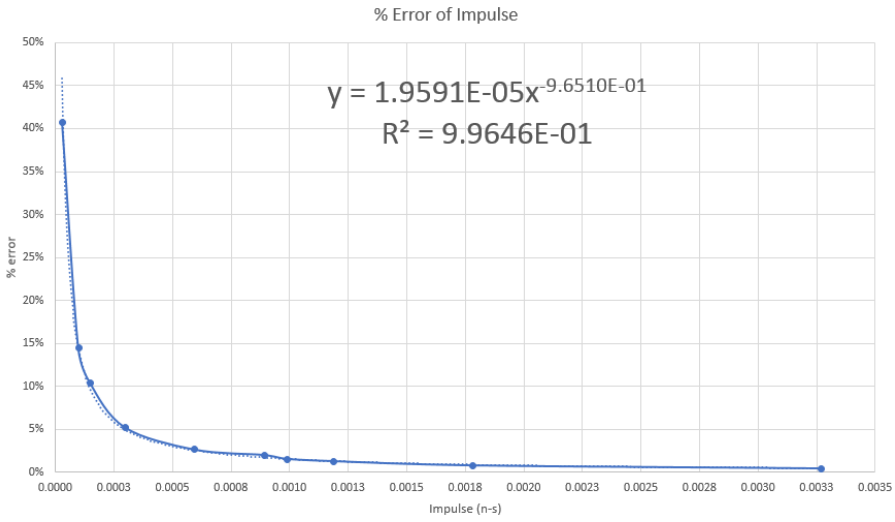

Fig. 28 Plotted percent error and impulse with trendline and R^2

The power function trendline fits the data well and thus can be used to estimate the percent of error in the impulse recorded by the thrust stand. As can be seen, the larger the impulse, the smaller the percent of error in the data. Assuming the threshold of acceptable error is about 10%, the minimum impulse the thrust stand can record is about 150 μN-s,

which is about half of the target impulse for this stand to record. Below this impulse the error can be seen to jump up very fast to the point where the noise overcomes the measurements of the LVDT.

The percent error can then be used to calculate a +/- value on the impulse. This is purely done by multiplying the inferred impulse by the percent error. Table 7 (overleaf), shows the percent error of the impulses inferred in this experiment, as well as the +/- values for each case.

Table 7 – Inferred Impulse with percent error and +/- error

Impulse (N-s)	% Error	+/- (N-s)
0.00326	0.49%	1.60424E-05
0.00189	0.83%	1.57401E-05
0.001168	1.33%	1.54777E-05
0.001052	1.47%	1.54217E-05
0.000919	1.67%	1.53488E-05
0.000691	2.20%	1.5197E-05
0.000332	4.46%	1.48128E-05

The calculated errors for the tested pendulums maximize at just under 4.5% which is well within tolerable error. These percent errors also help to account for the larger errors in the ratios previously calculated of inferred to expected impulse, recall Table 5:

Table 5 – Calculated and expected momentum with ratios

$L_{expected}$	$L_{thruster}$	L_{cw}	L_{total}	L ratio
0.0013074	0.00114	0.00017	0.0013041	0.99748
0.0007131	0.00069	6.3E-05	0.0007561	1.06028
0.0004754	0.00044	2.6E-05	0.0004671	0.98243
0.0003962	0.0004	2.1E-05	0.0004210	1.06265
0.0003566	0.00035	1.6E-05	0.0003676	1.03094
0.0002377	0.00027	9.3E-06	0.0002765	1.16309
0.0001189	0.00013	2.2E-06	0.0001327	1.11691

VI. CONCLUSION

The main objective of this thesis was to design a thrust stand that could measure a target impulse produced from a PPT. This target impulse was estimated to be 275 μN-s and in test conditions the fixture was capable to measure 332 μN-s ± 14.81 μN-s. The error analysis performed upon the fixture was aimed at the noise error from the sensor/conditioner. From this analysis, it can be inferred that the range of impulses tested are well within acceptable tolerance of under 5%. Additionally, it was estimated that the fixture could reliably record an impulse down to about 150 μN-s. Other errors that possibly affected the results of this test will not carry into actual thruster testing.

In the future, the fixture designed in this thesis can be upgraded with increased mechanical precision and less noisy electronics this may help to reduce the error observed. Thus, it can be concluded that the fixture designed over the course of this thesis is successful in recording the small impulse capable of being output by a PPT within an acceptable range of error.

REFERENCES

[1] NASA Glenn Research Center Fact Sheet-Pulsed Plasma Thruster, http://www.nasa.gov/centers/glenn/about/fs23grc.html

[2] Iio, J., Uezu, J., Fukushima, T., Kamishima, Y., and Takegahara, H., "Evaluation on Impulse Bit Characteristics of Pulsed Plasma Thruster by Single Impulse Measurement", The 29th International Electric Propulsion Conference, Princeton University, October 31- November 4, 2005

[3] Koizumi, H., Komurasaki, K., and Arakawa,Y., "Development of thrust stand for low impulse measurement from microthrusters." *Review of scientific instruments* 75.10 (2004): 3185-3190

[4] Haag, T. W., "PPT Thrust Stand," AIAA Paper 95-2917, *31st Joint Propulsion Conference*, 1995, see also NASA TM 107066.

[5] Wilson, M. J., Bushman, S. S., and Burton, R. L., "A compact thrust stand for pulsed plasma thrusters." *IEPC Paper* 97-122 (1997).

APPENDIX A

RAW LVDT PENDULUM DATA

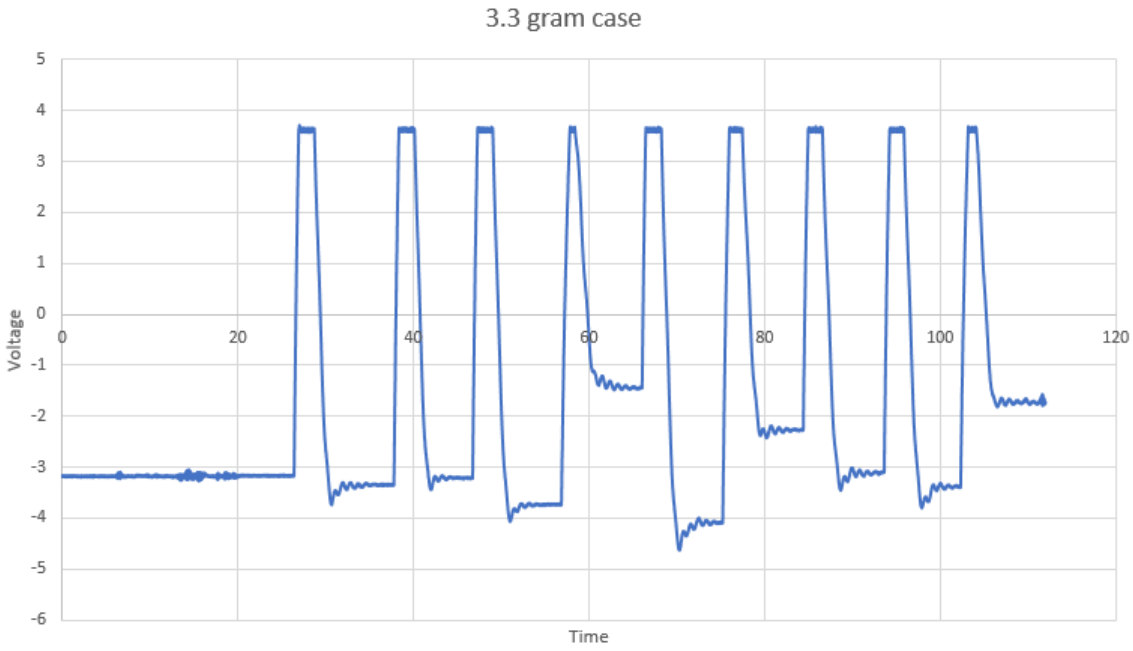
3.3 gram case
Voltage
Time
5
4
3
2
1
0
-1
-2
-3
-4
-5
-6
0
20
40
60
80
100
120

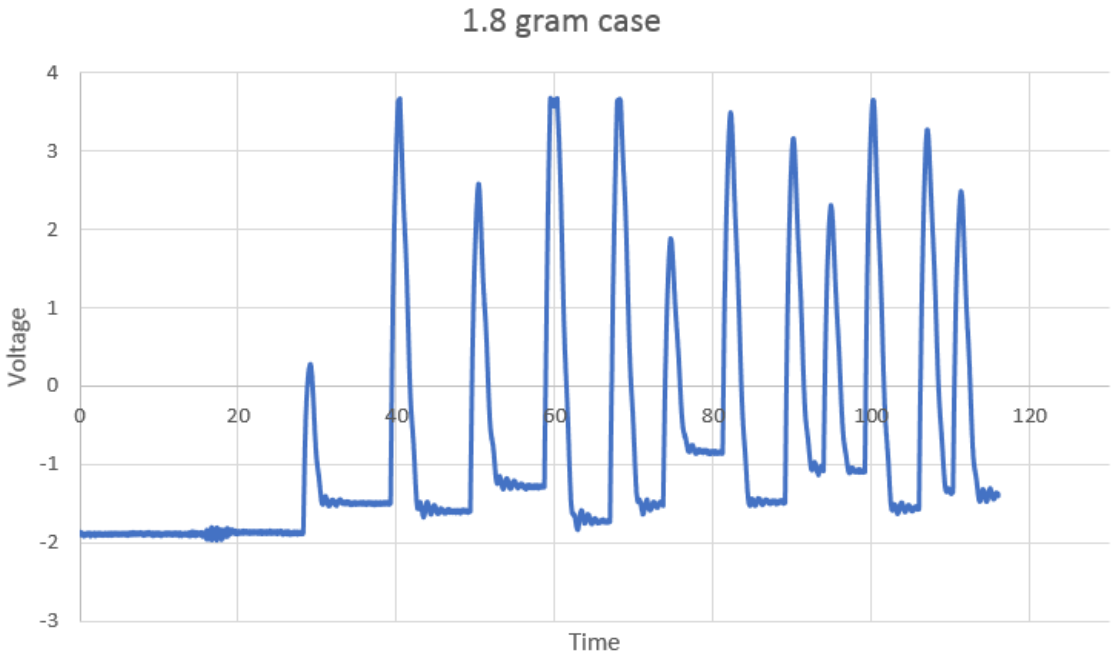
1.8 gram case
Voltage
Time
4
3
2
1
0
-1
-2
-3
0
20
40
60
80
100
120

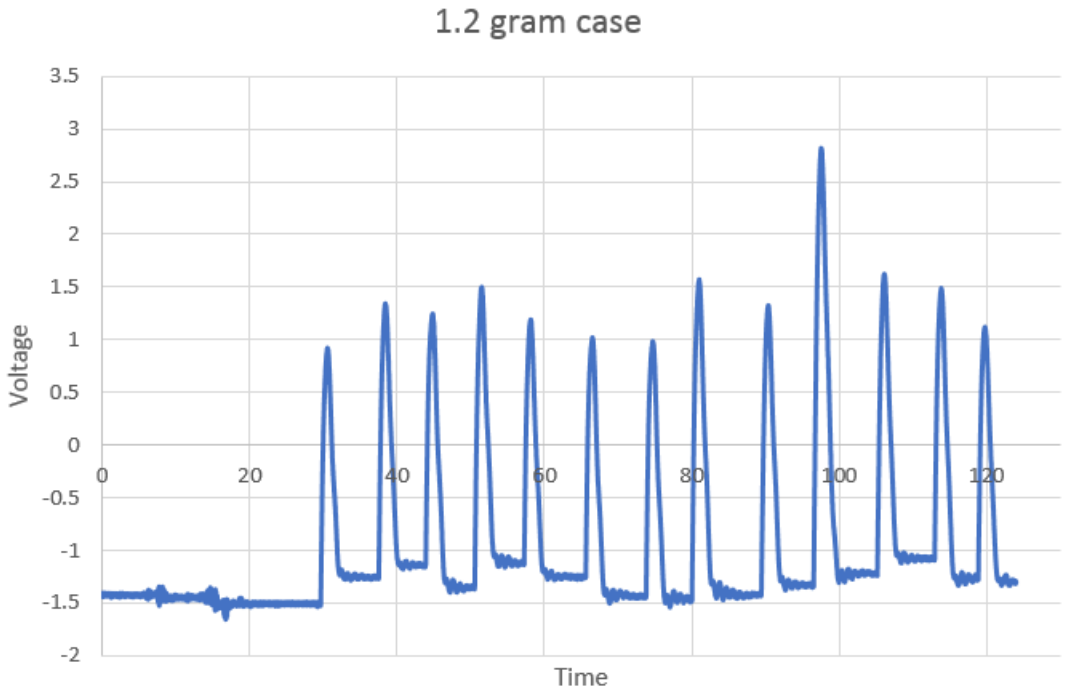
1.2 gram case
3.5
3
2.5
2
1.5
1
0.5
0
-0.5
-1
-1.5
-2
Voltage
0
20
40
60
80
100
120
Time

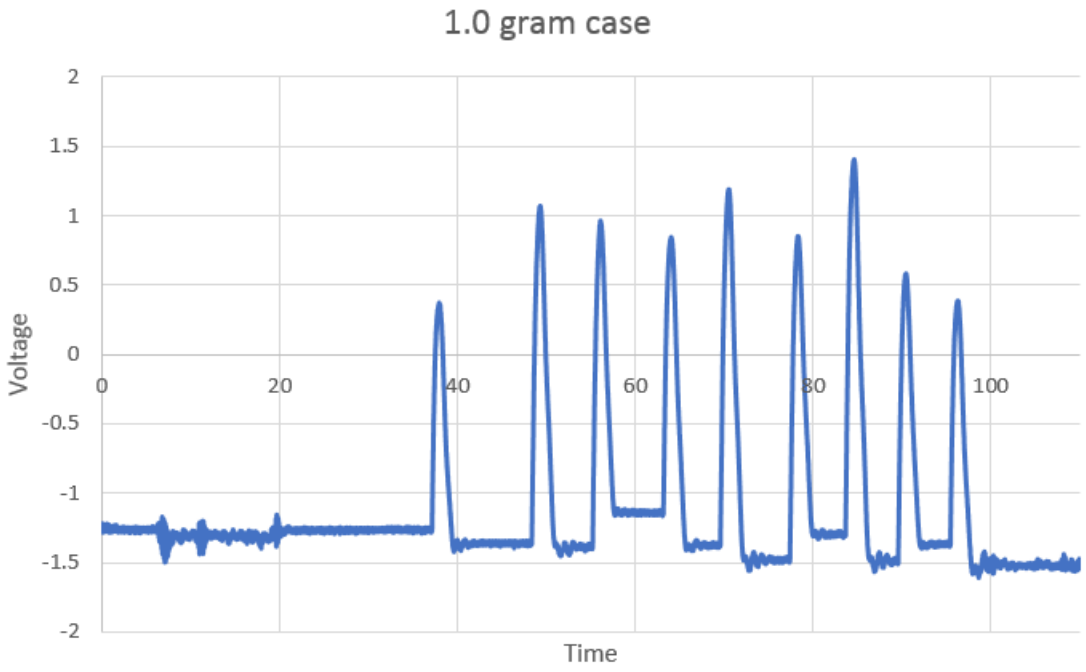
1.0 gram case
2
1.5
1
0.5
0
-0.5
-1
-1.5
-2
Voltage
0
20
40
60
80
100
Time

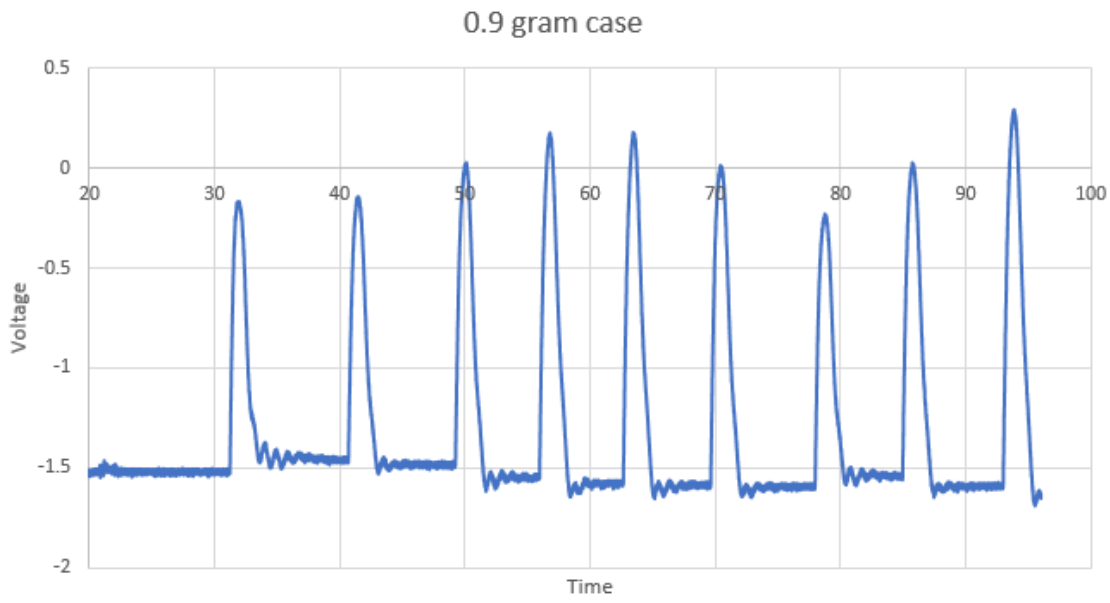
0.9 gram case
0.5
0
-0.5
-1
-1.5
-2
20
30
40
50
60
70
80
90
100
Voltage
Time

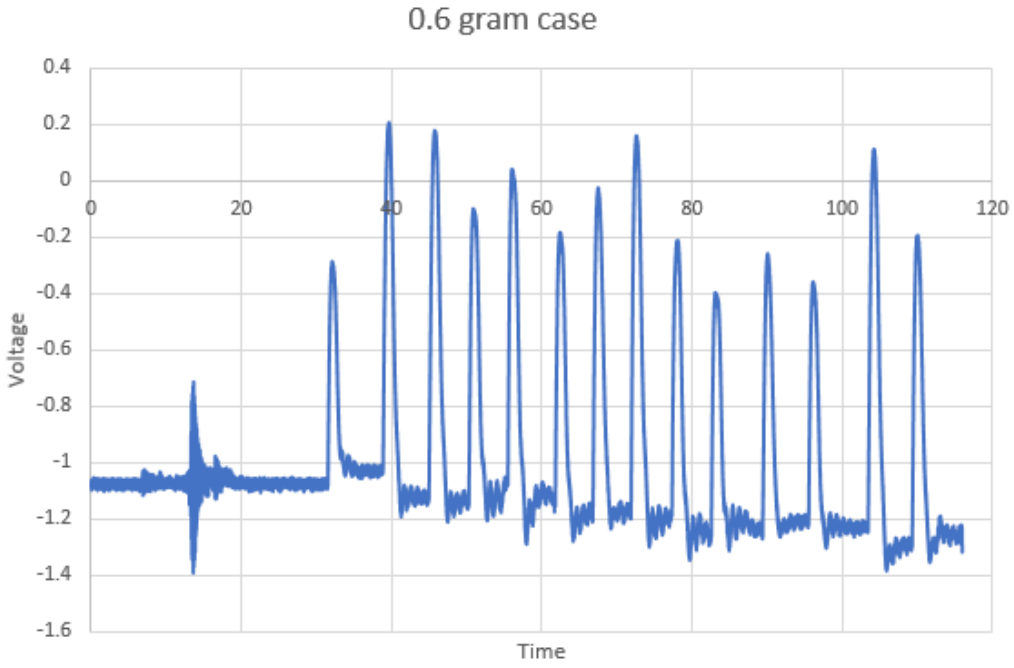
0.6 gram case
0.4
0.2
0
-0.2
-0.4
-0.6
-0.8
-1
-1.2
-1.4
-1.6
0
20
40
60
80
100
120
Voltage
Time

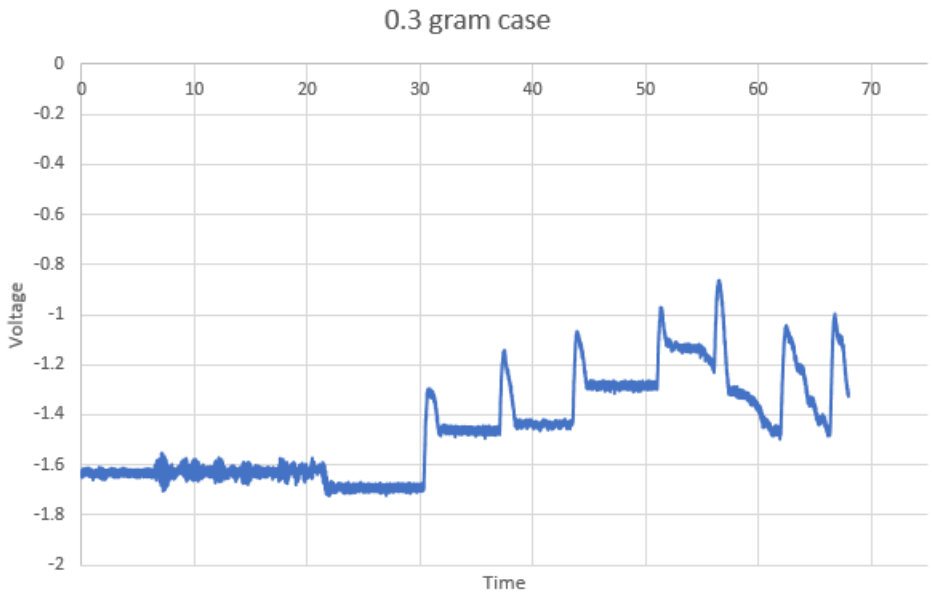
0.3 gram case
0
-0.2
-0.4
-0.6
-0.8
-1
-1.2
-1.4
-1.6
-1.8
-2
0
10
20
30
40
50
60
70
Voltage
Time

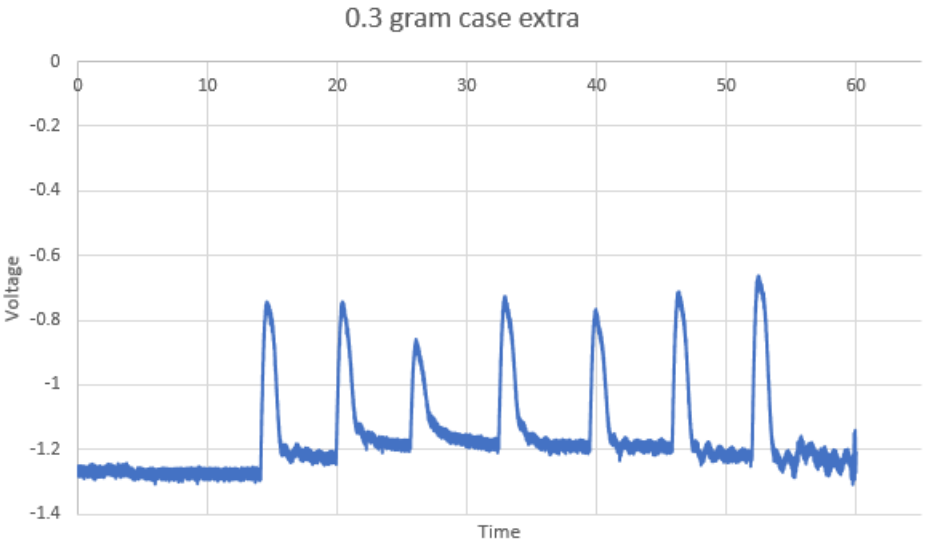
0.3 gram case extra
0
-0.2
-0.4
-0.6
-0.8
-1
-1.2
-1.4
0
10
20
30
40
50
60
Voltage
Time

APPENDIX B

RAW CALIBRATION LVDT DATA

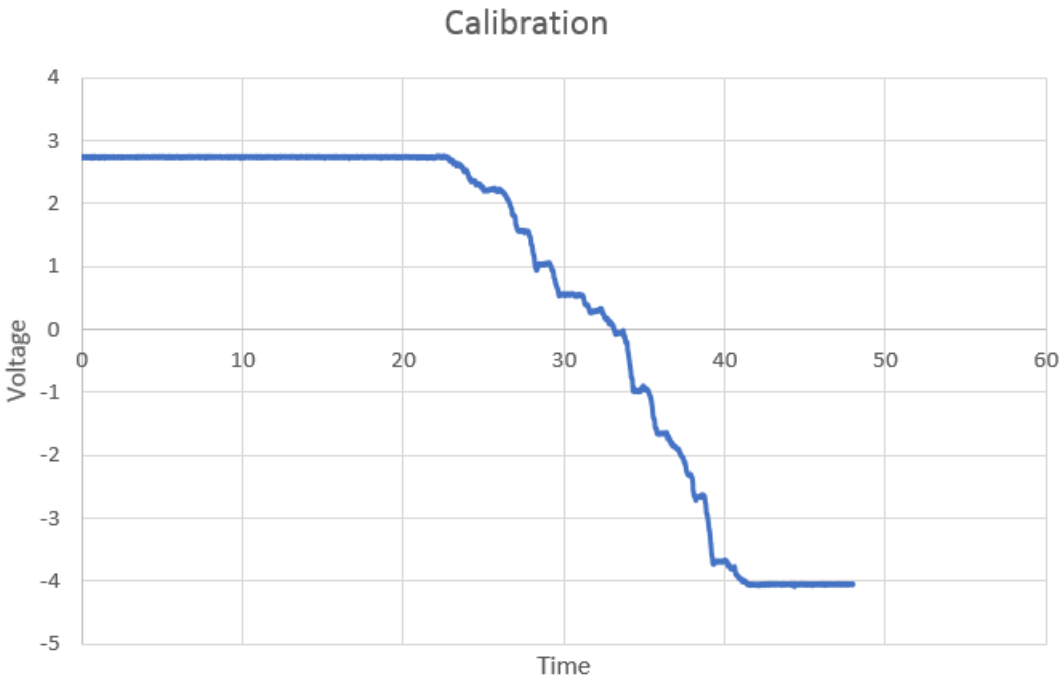
Calibration
Voltage
Time
4
3
2
1
0
-1
-2
-3
-4
-5
0
10
20
30
40
50
60